8-7-2004

Development of an Experimental Apparatus and Method for Characterizing the Leakage of Helium Gas through Composites Due to Cryogenic Operation

James Gordon Ragsdale

DEVELOPMENT OF AN EXPERIMENTAL APPARATUS AND METHOD FOR CHARACTERIZING THE LEAKAGE OF HELIUM GAS THROUGH COMPOSITES DUE TO CRYOGENIC OPERATION

By

James Gordon Ragsdale

A Masters Thesis
Submitted to the Faculty of
Mississippi State University
in Partial Fulfillment of the Requirements
for the Degree of Master of Science
in Mechanical Engineering
in the Department of Mechanical Engineering

Mississippi State, Mississippi

August 2004

DEVELOPMENT OF AN EXPERIMENTAL APPARATUS AND METHOD FOR CHARACTERIZING THE LEAKAGE OF HELIUM GAS THROUGH COMPOSITES DUE TO CRYOGENIC OPERATION

By

James Gordon Ragsdale

Approved:

W. Glenn Steele Professor of Mechanical Engineering and Department Head	Rogelio Luck Associate Professor of Mechanical Engineering Graduate Coordinator Department of Mechanical Engineering
Judy Schneider Assistant Professor of Mechanical Engineering (Major Professor)	Richard Patton Assistant Professor of Mechanical Engineering (Committe Member)
Steven R. Daniewicz Professor of Mechanical Engineering (Committe Member)	Robert Taylor Interim Dean of College of Engineering

Name: James Gordon Ragsdale

Date of Degree: August 7, 2004

Institution: Mississippi State University

Major Field: Mechanical Engineering

Major Professor: Dr. Judy Schneider

Title of Study: DEVELOPMENT OF AN EXPERIMENTAL APPARATUS AND METHOD FOR CHARACTERIZING THE LEAKAGE OF HELIUM GAS THROUGH COMPOSITES DUE TO CRYOGENIC OPERATION

Pages in Study: 68

Candidate for Degree of Master of Science

Carbon fiber composite cryogenic fuel tanks are very attractive to the aerospace industry. More information is needed on micro-cracking and how different composite formulations perform at cryogenic temperatures. In this study a cryogenic bulge test fixture was developed to rapidly screen small scale composite samples that are easily formulated in the laboratory. The design goal was to develop a simple fixture that induced thermal and mechanical strains in the same fixture. The pressure decay rate of helium gas through the composite sample after cryogenic operation gives a measure of the amount of micro-cracking induced. Uncertainty analysis techniques were employed to determine the resolution of the pressure decay determined from the bulge test.

ACKNOWLEDGMENTS

This work was supported by grant number #58404-511 from The Center for Advanced Manufacturing Louisiana Partnership. I would like to thank Dr. Judy Schneider for the valuable input and support you have given me. Public speaking was a character building exercise for me, but in the end I am better for it.

CONTENTS

CHAPTER Page

LIST OF TABLES

LIST OF FIGURES

CHAPTER I

INTRODUCTION

1.1 Project Motivation

Today's aerospace industry is looking for new technology to reduce the cost of launching payloads into orbit. A major factor to launch costs is the vehicle weight. Carbon fiber reinforced polymer (CFRP) matrix composite cryogenic fuel tanks have been proposed as an enabling technology for reducing the weight of launch vehicles. Carbon fiber has a higher stiffness to weight ratio than steel or aluminum and can be molded into complex shapes. This allows strong yet light structures that can be made as integral parts of the vehicle.

An example of a vehicle which uses a complex composite load bearing tank to decrease weight is the X-33 technology flight demonstration vehicle. This vehicle was a small scale technology demonstrator for development of the next generation space shuttle. This tank was highly innovative and technically advanced. It was made with a IM7 intermediate modulus carbon fiber and 977-2 toughened epoxy matrix. However, during testing the tank failed. One probable failure mechanism was micro-cracking of the inner face-sheet which lead to gaseous hydrogen (GH_2) infiltration of the structure of the tank [1]. The infiltration of the gas over pressurized the honey-comb core and caused the debonding

of the composite sheets bonded to the core. For carbon fiber composite cryogenic tanks to be used in the aerospace industry, designers need a better understanding of the micro-cracking phenomenon and its implications on tank design. One major aspect of cryogenic tank design that designers need to keep in mind was demonstrated by Aoki et al. [2] Their research showed that the onset of micro-cracking is drastically lower at cryogenic temperatures and decreases with decreasing temperature. This could cause a premature failure of the structure well before the ultimate failure of the composite as demonstrated by the X-33's CFRP tank.

1.2 Micro-cracks and Micro-crack Formation

Micro-cracking is a damage mechanism in carbon fiber composites where small cracks form in the polymer matrix. One cause of micro-cracking is a coefficient of thermal expansion (CTE) mismatch between the carbon fiber and the polymer matrix [3]. When the temperature is decreased the fibers contract in the radial direction and expand along the longitudinal axis while the matrix contracts in all directions [4]. This causes a residual stress in the ply at the fiber-matrix interface. When these stresses exceed the ultimate strength of the matrix, a micro-crack is formed to relieve the stress. Micro-cracks tend to propagate through the total thickness of a ply perpendicular to the fibers. Figure 1.1 shows a typical micro-crack in IM7/977-3. The crack has propagated all the way through the thickness of the ply causing a delamination at the interface of a differently angled ply. Generally the crack will propagate along the fiber matrix interface, but in some cases

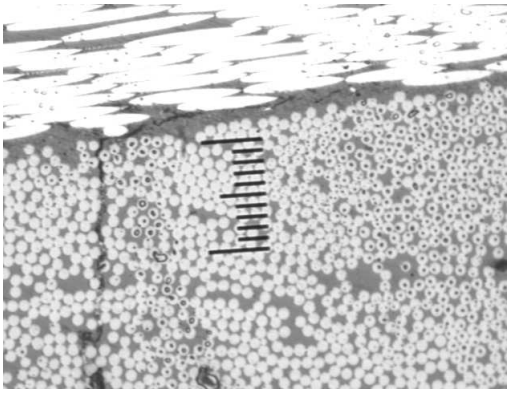

Figure 1.1 Micro graph of a transverse crack in IM7/977-3 (50μm scale)

where there is good fiber matrix adhesion, fiber splitting and crack bifurcation can occur [3]. Also micro-cracks tend to avoid resin rich areas [5]. In thick ply groups, two or more 0.127 mm plies of the same orientation, cracks tend to behave in the 'classical' manner, ie, the crack propagates through the thickness and width of the ply. Thin ply groups have short discontinuous cracks with a variation in the crack density over the ply [6]. It is therefore important that the crack detection method is matched with the lay-up sequence being investigated. For example with a $[0/-45/90/45/0]_s$ balanced symmetric lay-up, edge crack densities may not give a good correlation with the interior crack density.

For a micro-crack to form, the stress state in the matrix must exceed a critical value. Whether a laminate forms micro-cracks depends on the amount of thermal residual stress present, the amount of mechanical loading applied, the ply layup geometry, the fiber modulus, polymer fracture toughness, and the ultimate strength of the polymer matrix. Table 1.1 is a list of researchers who have experimental data on the performance of carbon fiber composites at cryogenic temperature. Half of the researchers only used thermal cy-

cling while the other half incorporated mechanical cycling as well. Depending on the composite properties or layup, mechanical loading may or may not be needed to drive micro-cracking. For example, Jae Noh et. al. [7] investigated a IM7/977-2 composite in a

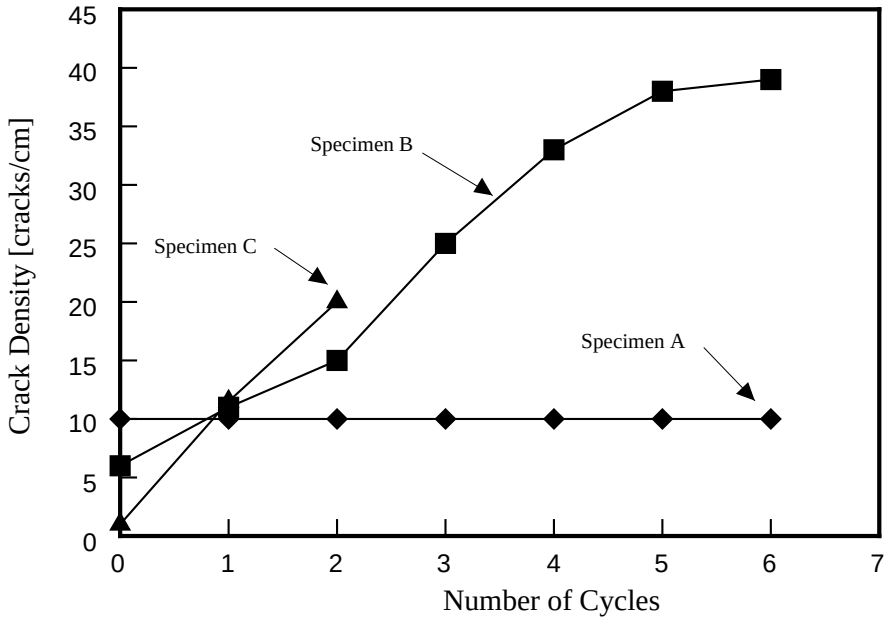

Figure 1.2 Micro-crack density versus number of cycles for IM7/977-2[7]

$[0/-45/90/45/0/45/90/-45/0]_s$ layup.

Table 1.1 Summary of cryogenic micro-crack performance evaluation

Reference	Matrix	Fiber	Applied Thermal Gradient	Applied Mechanical Loading	Layup
Knouff, Tompkins, and Jayaraman[8]	ERL 1939-3	T50, T55-5-s, T75-3, P100-s, P120-s	x		$[0/45/90/-45]_s$
Adams, Bowles, and Herakovich[5]	5208	T300	x		$[0/90_3]_S$, $[0_2/90_2]_S$,$[0_3/90]_S$, $[90/0_3]_S$, $[90_2/0_2]_S$
Park and McManus[6]	934, ERL1962	P75	x		$[0_2/90_2]_s$, $[(0/90)_2]_s$, $[0_2/\pm 30]_s$, $[0/45/90/-45]_s$, $[0/90/\pm 45]_s$, $[0/\pm 45/90]_s$, $[0_2/45_2/90_2]_s$
Aoki, et. al.[2]	$180°C$, $130°C$ cured epoxy, bismaleimide, PEEK	IM Carbon Fiber	x	x	$[0_2/90_2]_S$
Rivers, Sikora, Sankaran[9]	977-2	IM7	x	x	Sandwich Inner: $[45/90_3/-45/0_{1.5}]_s$ Outer: $[65/0/-65/90_{0.5}]_s$
Kim, Rice, Donaldson[10]	977-3, 5250-4	IM7	x	x	$[0_2/90_2]_s$, $[0/45/-45/90]_s$
Noh, et. al.[7]	977-2	IM7	x	x	$[0/-45/90/45/0_{0.5}]_S$
Kumazawa, Aoki, Susuki[11]	#133, #101	IM600		x	$(0_2/90_2)_s$

Table 1.1 Summary of cryogenic micro-crack performance evaluation cont..

Reference	Matrix	Fiber	Applied Thermal Gradient	Applied Mechanical Loading	Layup
McManus and Maddocks[12]	3501-6	AS4	x		$[0_4/45_4/90_4/-45_4]_S$, $[0_2/45_2/90_2/-45_2]_s$, $[0_2/60_2/-60_2]_S$
Nobelen, Hayes, Seferis[13]	Epoxy resin combination	T300	x		$[0_3/90_3]_s$
Schoeppner, Kim, Donaldson[14]	977-3	IM7	x	x	[0/90_2/0], [0/90_3/0], $[0_2/90_2]_s$
Bechel et. al.[15]	5250-4, 977-3	IM7	x		$[0/90]_{2s}$, [0/45/-4590]$_s$, [(90/0)$_4$/90]

Figure 1.2 shows the micro-crack density as a function of cycles for the second ply [-45] from the surface of the laminate. Sample A was subjected to 20 thermal cycles and did not show an increase in crack density. Specimen B was was subjected to thermal cycling and mechanical loading at room temperature. The micro-crack density stabilized at about eight times the initial damage. Specimen C was mechanically loaded at cryogenic temperature. Specimen C had the highest damage increase rate, but the test had to be halted when the specimen delaminated in the grips. On the other hand, Knouff, Tompkins, and Jayaraman [8] thermally cycled cyanate ester composites and showed an increase in micro-crack density. Figure 1.3 shows the micro-crack density in a T50/ERL1939-3 with a [0/45/90/-45]$_s$ layup.

1.3 Matrix Modification for Improved Cryogenic Performance

Some research has been done to investigate how different aspects of the composite formulation affect the micro-crack density in the composite after mechanical loading with thermally induced residual stresses. Timmerman et al. [16] investigated the effect of fiber modulus and matrix morphology on the low temperature behavior of epoxy/carbon fiber laminates. Cross ply laminates in a $[0_3/90_3]_s$ stacking sequence were cycled between $22°C$ and a liquid nitrogen bath (-196°C) for 10 minutes. After exposure to the liquid nitrogen, the samples were placed in a desiccator to return to room temperature. After each thermal cycle optical microscopy was used to calculate the edge crack density for each sample. Using a combination of resins and hardeners they were able to vary the

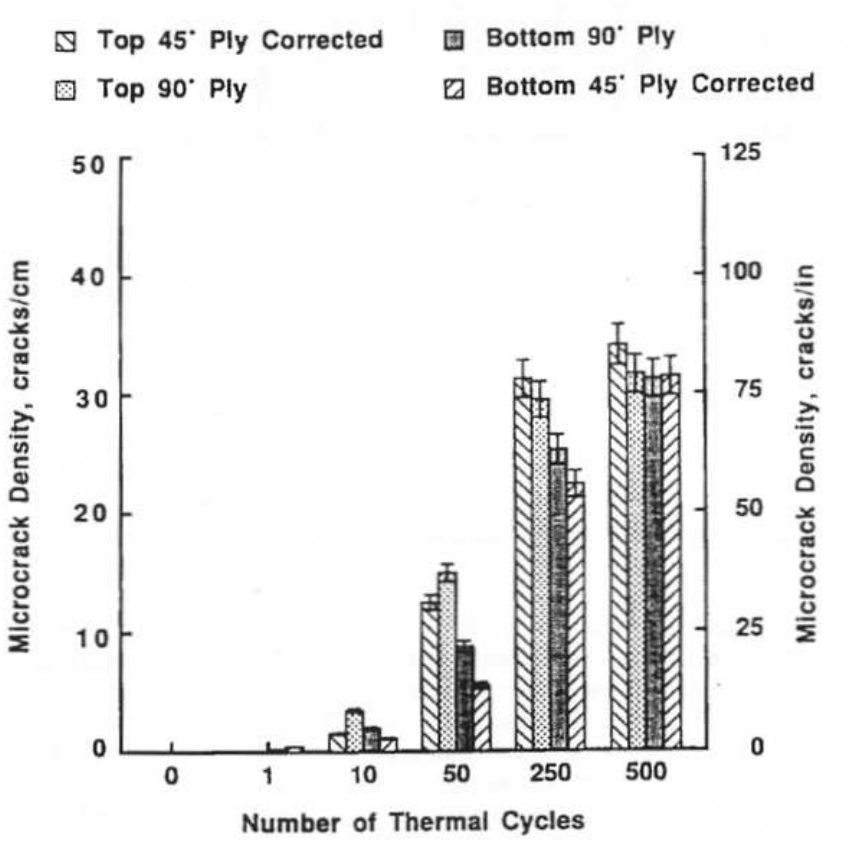

Figure 1.3 Micro-crack density versus the number of cycles for T50/ERL1939-3[8]

glass transition temperature (T_g) of the resin. They observed that resins with lower glass transition temperatures had higher crack densities after thermal cycling. Their research showed that for a given resin system, a lower T_g corresponds to a higher CTE [17]. This will lead to an increased micro-crack density. Figure 1.4 shows how the micro-crack density varies with T_g as reported by Timmerman et al [16]. Judging from Figure 1.4, a correlation between the T_g and the micro-crack density may not be appropriate. There are only two points for T_g's over 100°C and the micro-crack densities corresponding to the T_g's below 100°C show considerable scatter. More testing needs to be done before the T_g can be related to the micro-crack density. Figure 1.5 show the effects of fiber modulus on the crack density. Low, medium, and high modulus fibers were thermally cycled and the micro-crack density increased with increasing modulus.

The addition of nano-scale particles to the resin is a promising means of improving the cryogenic performance of CFRPs. Ganguli et. al. [18] and Timmerman et. al. [3] both investigated the changes in performance of thermosetting resins with the inclusion of small amounts of highly dispersed modified montmorillonite clay. Ganguli et. al. [18] focused on the improvement of thermal and mechanical properties of a nano modified cyanate ester. Table 1.2 is a summary of their results showing the improvement in physical properties. The decrease noted in CTE has been cited as a possible way to improve the composites resistance to micro-cracking. Timmerman et. al. [16] studied an epoxy resin formulated from EPON 828 and Araldite MY 9512 cured with HT 976 diaminodiphenyl sulfone (DDS) in a $[0_3/90_3]_s$ lay-up. They looked at the micro-crack density as a function

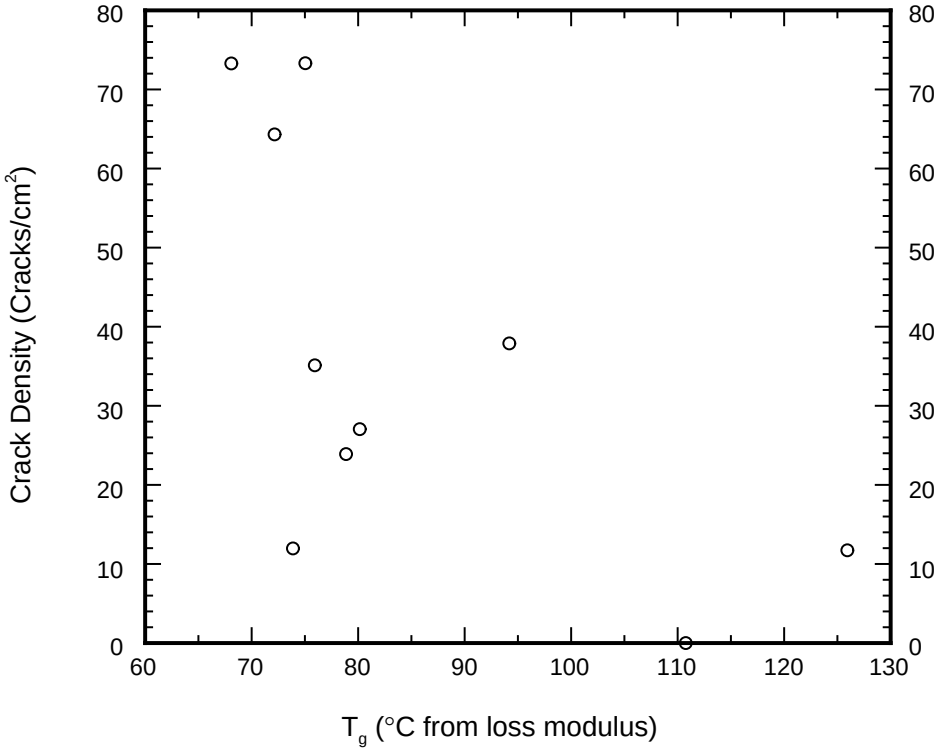

Figure 1.4 Micro-crack density versus laminate glass transition temperature[16]

Table 1.2 Physical properties of cyanate ester/layered silicate nano-composite[18]

	Neat	Cloisite 30B		
		1%	2.5%	5%
$K_{Ic}(MN/m^{3/2})$	0.62	0.72	0.85	0.89
E (GPa)	2.9	3.7	4.5	4.3
Strength(MPa)	173	179	185.2	186
$T_g°C$	305	329	378	390
CTE(μm/m $°C$)	60	50	46	44

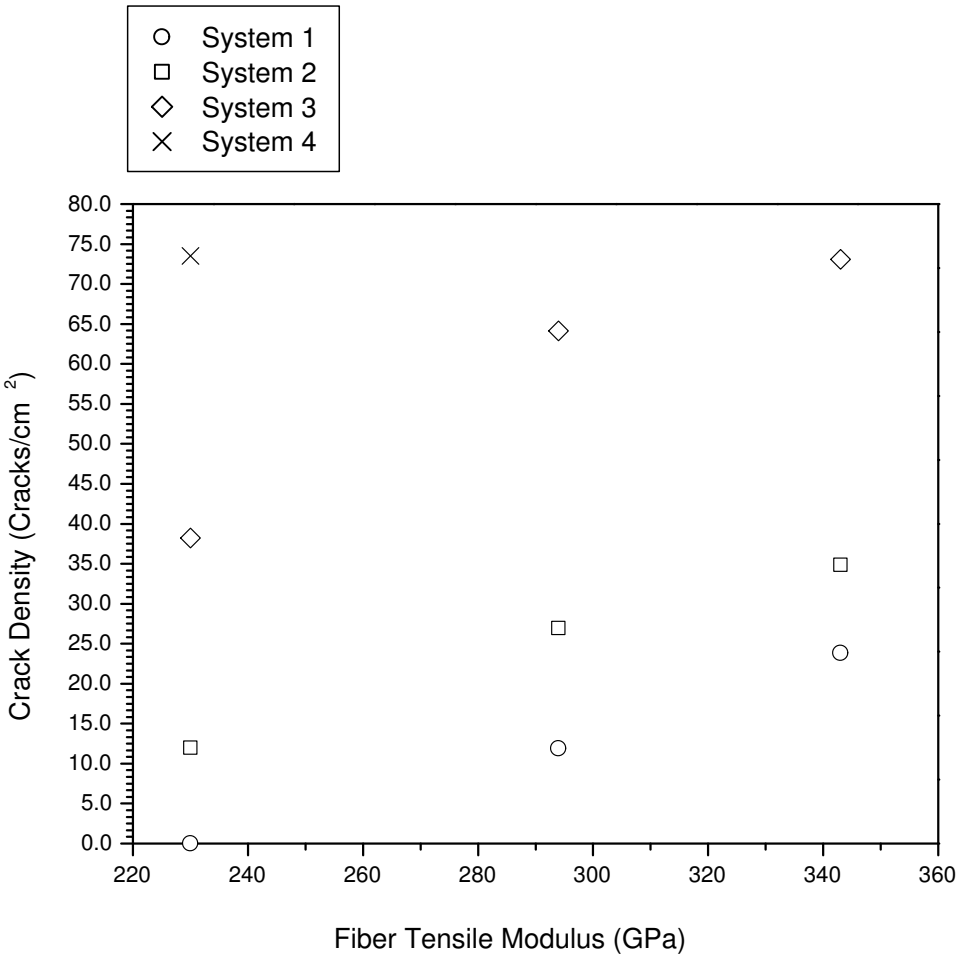

Figure 1.5 Crack density variation with fiber type[16]

of the type of filler and concentration. Figure 1.6 shows the variation in micro-crack density for the 5phr Alumina and 2, 5, and 8phr montmorillonite clay. The cited advantages for nano-scale modifiers is the improvement in physical properties, decrease in permeability, and resistance to micro-cracking [18, 3]. The disadvantage is the increased difficulty in processing. The advantages depend on the nano-scale modifiers being highly dispersed or exfoliated in the matrix [19].

Another promising means of reducing the micro-crack density is with the addition of rubber tougheners. Nobelen, Hayes, and Seferis [13] investigated the effects of matrix tougheners in relation to micro-cracking using three different types of matrix toughening, interlayer toughening using 50μm preformed rubber particles, 0.3μm core shell dispersed phase toughening, and continuous phase toughening. They used a combination of epoxy resins to yield a high temperature aerospace-grade epoxy to which different combinations of the tougheners were added at a concentration of 6 phr. The 50μm rubber particles and the 0.3μm core shell are dispersed in the matrix while the rubbers used in the continuous phase toughening must be dissolved in a solvent before mixing in the resin. These resins were prepreged with Toray T300 12K epoxy sized fibers to make a $[0_3/90_3]_S$ layup. Figure 1.7 shows the micro-crack density for each of the resin types after exposure to cryogenic cycling. A cycle consisted of submerging the composite sample in liquid nitrogen for ten minutes. All samples were cycled a minimum of five times or until optical microscopy indicated no new micro-cracks appeared. The continuous phase toughening

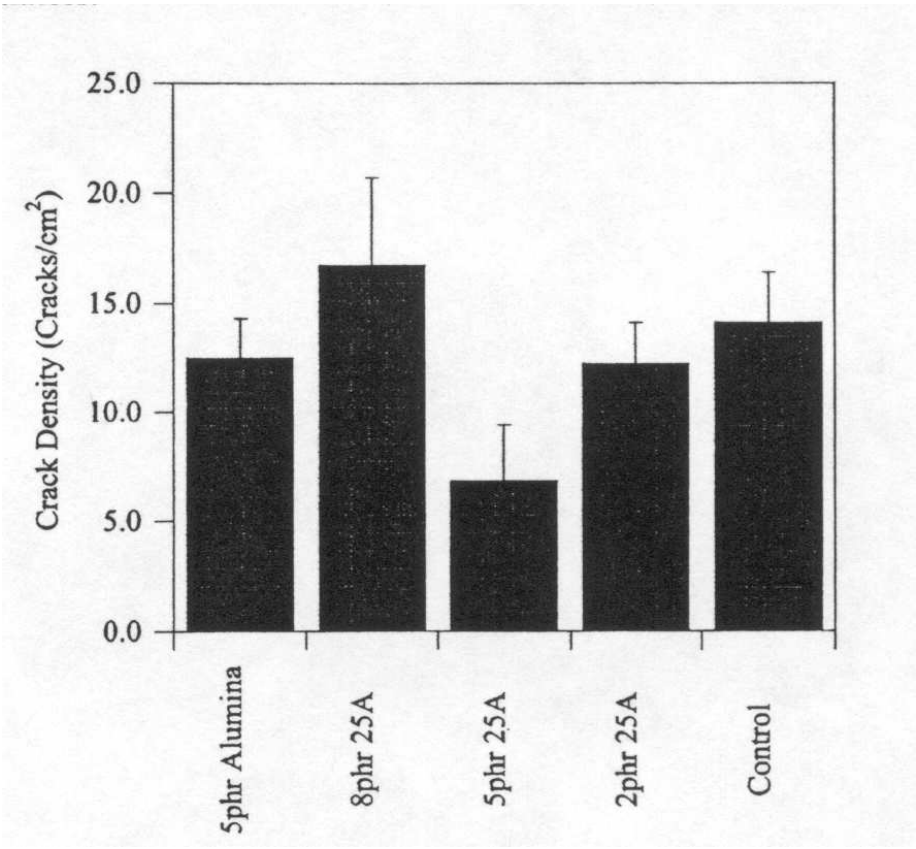

Figure 1.6 Crack density variations with particle modification[3]

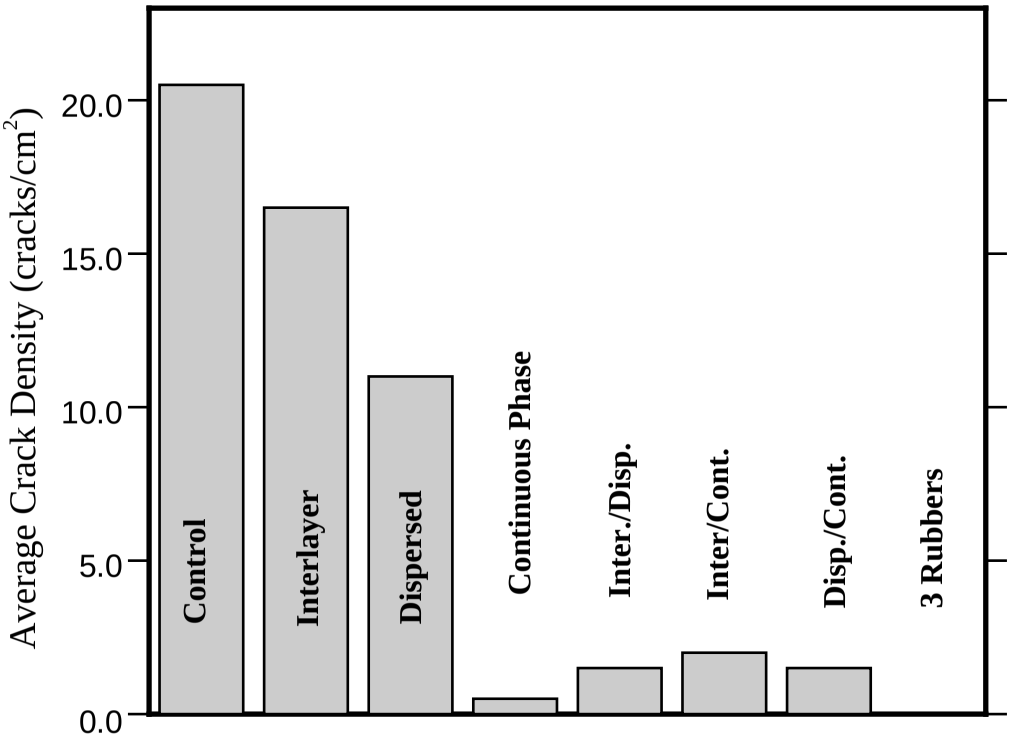

Figure 1.7 Average crack density of the toughened laminates after cryogenic cycling[13]

displays the best performance for a single additive while higher concentrations of rubber tougheners showed improved performance.

1.4 Thermoplastics Improved Cryogenic Performance

Another possible solution to reducing the micro-cracking problem is to change from a thermosetting (TS) to a thermoplastic (TP) resin. Most polymers exhibit a linear stress-strain relation and have a low fracture strain at cryogenic temperature. The static fracture strain ϵ_{UTM} at 4.2K for most TS polymers does not exceed 2% [20]. However, some linear TPs such as PC, PSU, PES, and HPDE exceed 2% strain even at 4.2K. This increased fracture strain is due to the absence of cross linking in a TP. This allows the polymer chains to slide along one another. Hartwig[20] defines free strain

$$\epsilon_m^f = \epsilon_{UTM} - \epsilon_m^R \tag{1.1}$$

where

$$\epsilon_m^R = \alpha \Delta T \tag{1.2}$$

is the thermal strain induced by the temperature gradient and ϵ_{UTM} is the fracture strain. The free strains can be seen for various polymers in Table 1.3. Free strain equates to the amount of mechanical strain that the polymer will tolerate before fracture. Table 1.4 shows the mechanical properties of different carbon fibers including their strain to failure. Because the strain to failure of the thermoplastic is larger than the fibers, micro-cracking maybe less prone to develop.

Table 1.3 Thermal strain data for various neat resins[21]

Resin	Fracture Strain (%) (293K-4.2K)	Thermal Strain (%) (293K-4.2K)	Free Strain (%) (293-4.2K)
Polysulfon[20]	3.2	1.1	2.1
HDPE[20]	3.5	1.8	1.7
PC[20]	3.5	1.4	2.1
EPON 828 Epoxy[20, 22]	<1.6	1.1	<0.5

1.5 Summary

Although composites have been investigated for cryogenic applications for over 20 years, it is only recently that advanced aerospace composites have been investigated for cryogenic tank applications [24]. The different formulations of composites need to be investigated and statistically evaluated for low temperature performance. NASA is currently looking at IM7/977-3 as a suitable composite system for cryogenic use. Its cryogenic performance needs to investigated. Baselining IM7/977-3 will serve as a basis to evaluate modified resins for improving cryogenic performance.

This thesis will present the development of the bulge test, a relatively inexpensive and quick method for evaluating the cryogenic performance of polymer matrix composites. This test fixture will be used to investigate IM7/977-3 hand layup using pre-preg fibers, IM7/977-3 using a wet layup, AS4/PEEK hand layup using pre-preg fibers, and IM7/977-3 wet layup with clay modifiers added to the resin. Current data will be presented for these material types for the bulge test, volume fraction, density, and room temperature tensile data.

Table 1.4 Carbon fiber properties

Fibre	Type	Tensile strength [MPa]	Strain to failure [%]	Tensile Modulus [GPa]
Torayca T300[23]	HT	3100	1.30	230
Hercules AS4[23]	HT	3800	1.69	230
Torayca M40[23]	HM	2500	0.60	400
Cytec/Fiberite IM7[24]*	IM	3999	1.6	228

*Filament diameter: 5 microns

CHAPTER II

EVALUATION OF DAMAGED INDUCED LEAKAGE

2.1 Bulge Test Development

2.1.1 NASA's Bulge Test Program

NASA has developed a bulge test for evaluating composites for cryogenic performance. Based at Marshall Space Flight Research Center, the test uses a large 24 inch panel that is cooled with liquid hydrogen. Gaseous helium is used to bulge the panel to 7000$\mu\epsilon$ and the mass flow of the helium through the composite panel is measured. To achieve effective sealing at 4.2K, expensive non-reusable seals are used. This process is costly and cannot be used to screen many different formulations. The bulge test developed in this study is relatively inexpensive and quick to compliment the NASA test method.

2.1.2 Bulge Test Concept

The goal of the present bulge test is to provide a quick and inexpensive way to screen composites for the development of micro-crack networks developed by thermal and mechanical cycling by comparing the leakage rate of helium gas through the specimen. Key requirements are as follows:

- Small test samples with minimum fabrication required

- All parts need to be able to perform at liquid nitrogen temperatures -196°C
- Simple design
- Ability to develop thermal and mechanical strains with the same fixture
- Inexpensive seals

The bulge test fixture uses helium gas to pressurize a chamber on one side of the specimen which causes it to bulge like a diaphragm. This will impart biaxial tension into the sample and account for the mechanical strain. The fixture will be submerged in liquid nitrogen to induce the thermal strain in the sample. To quantify the amount of micro-cracking induced by the mechanical and thermal strain, the fixture will be charged with helium and the inlet and outlet valves will be closed. This creates a constant volume where the pressure decay of the helium indicates the amount of micro-cracking present in the sample. Figure 2.1 is a schematic diagram showing the cross section of the test sample. The sample is 2in square and 9 plies thick (about 0.042in). The pressure acts over a circle of $r = R_o$ where $R_0 = 0.75$in and the edges are fixed. The pressure is set to deflect the sample a distance of *h* measured at the center of the sample.

2.1.3 Design Features

The bulge test fixture has several key design features and are listed as follows:

- All parts that operate at low temperatures are made of FCC (Face Center Cubic) materials in order to avoid a ductile to brittle transition.
- Teflon O-Ring seals were used for all pressure ports including the composite sample to fixture seal.
- Valves on the pressure inlet and exit allow the cycling of pressure to induce mechanical work in the composite sample.

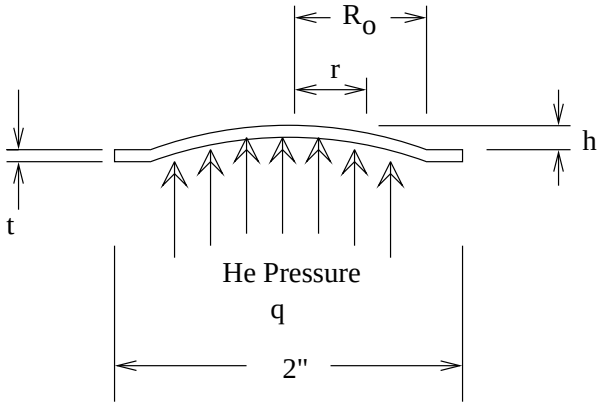

Figure 2.1 Bulge test schematic

- Computer controlled data acquisition of pressure, temperature, and strain.
- Temperature measurement to ensure that temperature fluctuations do not influence the pressure reading.

Figure 2.2 shows an assembly view of the test fixture.

2.1.4 Pressure, Strain, and Deflection Correlation

The first step in testing a composite sample in the bulge tester is to correlate the pressure and strain in the sample as a function of the deflection *h*. A sample with a strain gage bonded to the face is loaded into the bulge tester. A dial indicator is mounted to the fixture and positioned over the sample to measure the deflection. The strain and deflection are measured at the center of the sample. Figure 2.3 shows a plot that correlates the pressure, strain, and deflection for a sample from lot A001 which is a 977-3/IM7 hand layup. For this material, deflection is set at 0.025 inches in order to obtain 2700$\mu\epsilon$. This strain level was selected from the stress Aoki[2] reported for a $180°C$ cured epoxy laminate with in-

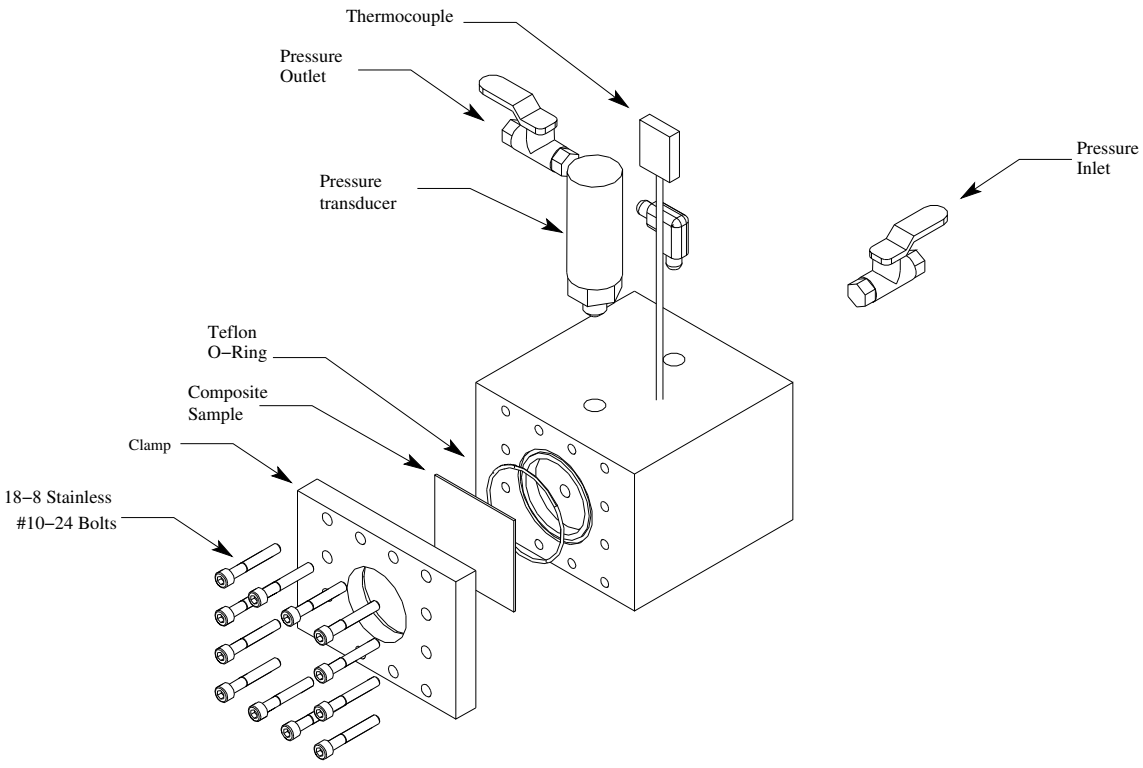

Figure 2.2 Assembly view of the bulge test fixture for evaluation of 2in x 2in composite samples

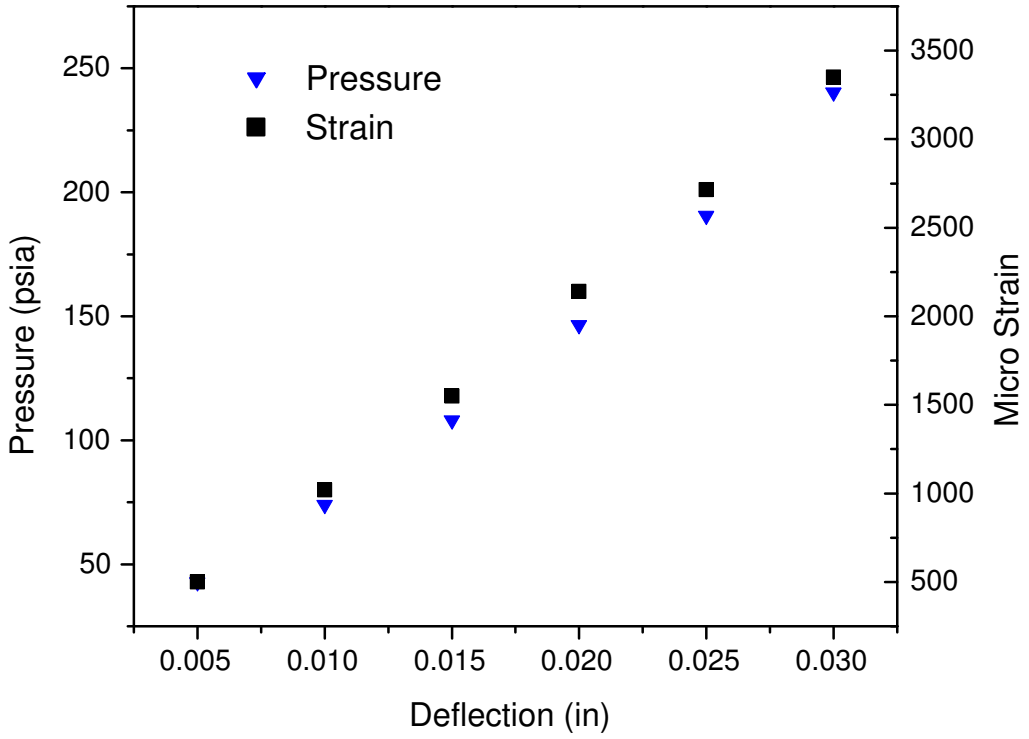

Figure 2.3 Bulge test correlation of pressure, deflection, and strain

termediate modulus fibers to induce micro-cracking at liquid nitrogen temperatures. For each sample, the pressure is adjusted to reach the correct deflection.

2.1.5 Decay Rate Data Collection

A sample is loaded into the fixture and the pressure is set using the dial indicator for a deflection found in Section 2.1.4. When the correct pressure is reached, the dial indicator is removed and the test chamber is sealed by closing the valves. The bulge test fixture is then placed in a water bath to control the temperature variations in the pressure control volume. The fixture is isolated from the water using a plastic barrier. This allows the water to control the temperature without wetting the specimen. These temperature variations can effect the pressure reading if not properly controlled. The pressure is then recorded for 90 minutes. Five pressure decay recordings are made with out changing the setup and averaged together. This gives a pressure decay rate for the undamaged composite sample. Next the fixture is submerged in liquid nitrogen and allowed to reach equilibrium temperature which takes about 15 minutes. This induces the thermal strain in the sample. Mechanical loading is provided by cycling the pressure for the desired number of cycles. The duration of each cycle is set at 2 seconds. The fixture is then allowed to warm and placed in the water bath to reach room temperature. This process takes about 8 hours. The pressure is reset to the initial pressure and the decay rate is again recorded over 90 minutes. Five pressure decay readings are taken and averaged together. The fixture is re-pressurized

between each test. This gives a pressure decay rate for the damaged composite sample. Figure 2.4 is a schematic drawing showing the test process.

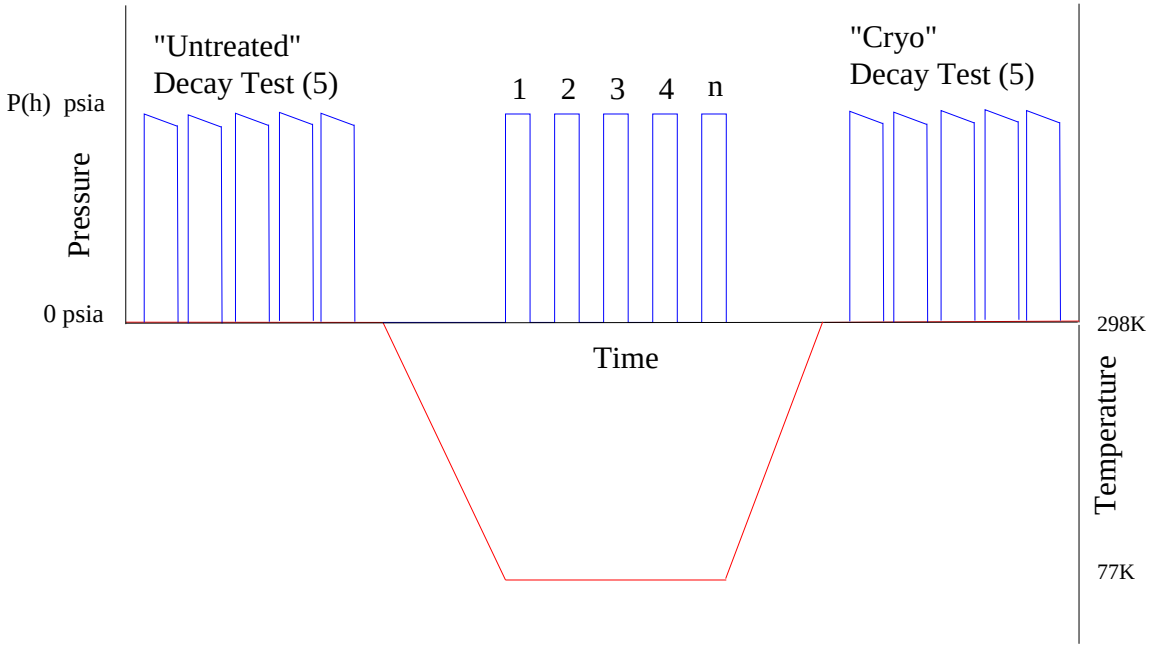

Figure 2.4 The bulge test procedure

2.1.6 Decay rate analysis

The data recorded in Section 2.1.5 is curve fitted using a linear line fit. Figure 2.5 shows an example of how the linear fit approximates the data. The slopes of the damaged and undamaged decay rates are then calculated. The corrected slope is calculated using Equation 2.1. The undamaged slope is then subtracted from the damaged slope to isolate the leakage due to the micro-cracking from the leakage due to the fixture.

$$M_{corrected} = M_{cryo} - M_{untreated} \tag{2.1}$$

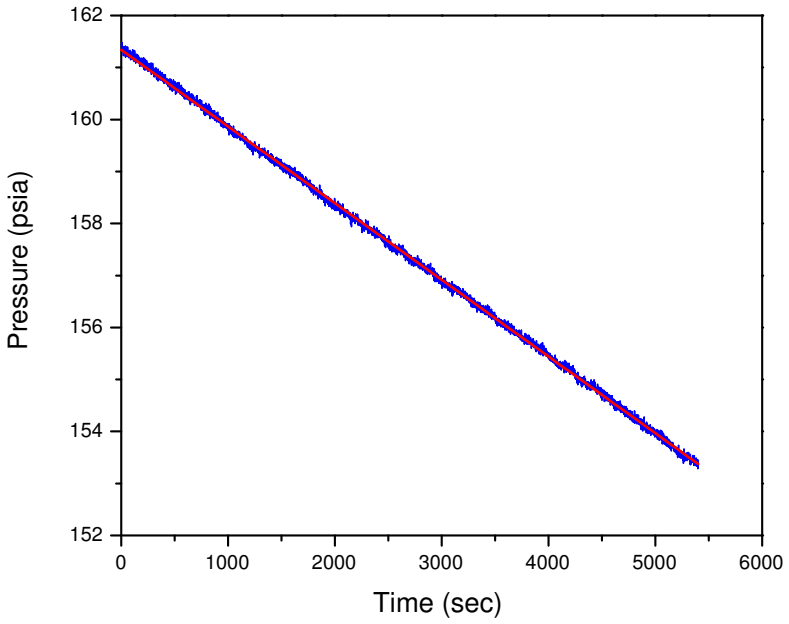

Figure 2.5 Example plot showing the linear line fit over recorded data for the second "Cryo" run of A008.2

The corrected decay rate is then recorded for each sample.

2.2 Uncertainty in pressure decay testing

2.2.1 O-Ring durability

One of the key assumptions in the pressure decay testing using the bulge test fixture is the ability of the O-Ring to withstand the cryogenic cycling and return to full effectiveness after warming to room temperature. In order to evaluate this a polished steel sample was installed in the bulge test fixture. This will isolate leakage to only that caused by the O-Rings or other fittings in the test fixture. For this testing, a number of pressure decay runs were collected for a new O-Ring that has not been subjected to liquid nitrogen. The fixture was then submerged in liquid nitrogen and allowed to cool to equilibrium temperature. The pressure was cycled ten times to simulate the pressure cycling done during testing. The fixture was then allowed to warm to room temperature and then more pressure decay runs were collected. Figure 2.6 shows the variation in the pressure decay before and after cryogenic treatment. Due to the uncertainty of the pressure decay after cryogenic treatment, any change in the decay is not detected.

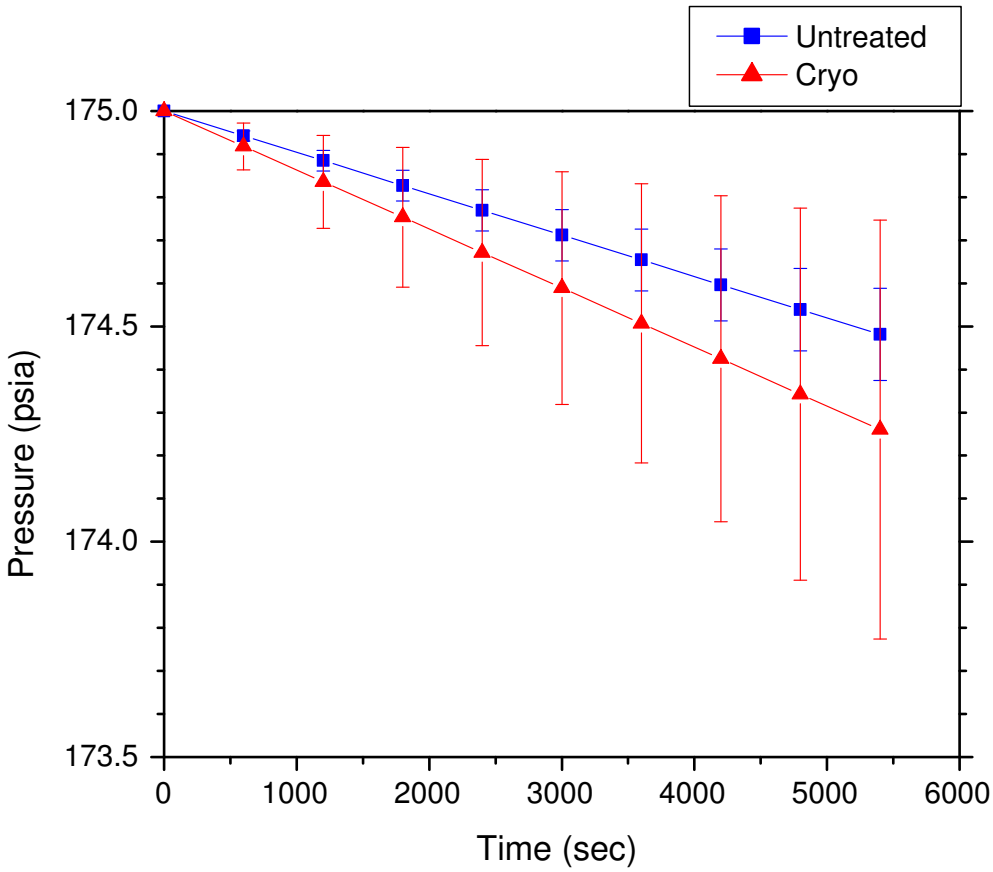

Figure 2.6 O-Ring assessment run

2.2.2 Uncertainty of the Decay Rate

The first aspect of uncertainty to investigate is the random uncertainty due to the linear regression used to calculate the slope. From Coleman and Steele[25], the uncertainty in the slope is given by the equation

$$S_m = \left(\frac{S_Y^2}{S_{xx}} \right)^{1/2} \tag{2.2}$$

where S_y is the standard error of regression and S_{xx} is as follows:

$$S_{xx} = \sum_{i=1}^{N} X_i^2 - \frac{\left(\sum_{i=1}^{N} X_i \right)^2}{N} \tag{2.3}$$

The standard error of regression given by the equation,

$$S_Y = \left[\frac{\sum_{i=1}^{N} (Y_i - mX_i - c)^2}{N-2} \right]^{1/2} \tag{2.4}$$

is an estimate for the standard deviation in the Y_i values for no uncertainty in the X_i values. In this case, the X_i values are time and have very small uncertainty so the uncertainty can be assumed to be zero.

The standard error of the slope gives a measure of how well the linear fit matches the data. The standard error of the slope for each pressure decay run can be seen in the data sheets in Appendix A. These uncertainty values are all less than 1% for all but a few decay runs which means that a linear fit is a good correlation to the data.

For each set of data, Untreated and Cryo, a mean is calculated to determine the slope that will be used in the corrected pressure decay. From Coleman and Steele[26], the random uncertainty of the mean is calculated using

$$P_m = \frac{tS_x}{\sqrt{N}} \tag{2.5}$$

where *t* is from the Student's t distribution. To calculate t, the effective number of degrees of freedom need to be calculated. It can be approximated using the Welch-Satterthwaite formula[27]:

$$\nu = \frac{\left(S^2 + S_B^2\right)^2}{S^4/\nu_S + S_B^4/\nu_B} \tag{2.6}$$

where ν_S is the number of degrees of freedom associated with the random error S and is given using the following equation:

$$\nu_S = N - 1 \tag{2.7}$$

ν_B is the number of degrees of freedom associated with the standard deviation estimate for the systematic uncertainty S_B. The standard deviation estimate for the systematic uncertainty is half the bias. The number of degrees of freedom is estimated using

$$\nu_B \approx \frac{1}{2}\left(\frac{\Delta B}{B}\right)^{-2} \tag{2.8}$$

where the quantity in parentheses is the relative uncertainty of the bias error. Equation 2.6 gives approximately 200 degrees of freedom so t is set to a value of 2.

The random uncertainties calculated using Equation 2.5 for the Untreated and Cryo slopes are used to calculate the uncertainty of the corrected slope with the following equation:

$$U_{mc} = \sqrt{P_{mc}^2 + P_{mu}^2} \tag{2.9}$$

In this case, the uncertainty is totally random. It can be shown using Coleman and Steele[27] that the bias error does not effect the slope. Since the bias is always the same, it will only shift the line and will have no effect on the slope.

CHAPTER III

STRESS ANALYSIS OF THE BULGE TEST SPECIMEN

Stress is a convenient quantity to use when discussing the ability for a material to meet an engineering objective. Knowing the stress state of the composite sample in the bulge test would be advantageous when discussing and comparing micro-crack performance with other researchers. Also the stress can be used in failure criterion such as the Tsai-Wu and the Maximum Stress Criterion[4]. The stresses in the bulge test specimen were investigated using a combination of finite element analysis and experimental strain gage measurements.

3.1 Material Properties

To determine the stresses in a composite laminate for the strains, the material properties of the individual plies need to be known. Table 3.1 lists the properties of IM7/977-3 carbon fiber epoxy acquired at both room temperature and liquid nitrogen temperature (-196$^{\circ}C$) reported by Schoeppner, Kim, and Donaldson[14]. Kim, Rice, and Donaldson[10] also reported the properties of IM7/977-3 carbon fiber epoxy at room temperature, liquid nitrogen temperature, and elevated temperature. These values are listed in Table 3.2.

Table 3.1 IM7/977-3 Material Properties[14]

	$23°C$	-196$°C$
E_1	172 GPa	179 GPa
$E_2 = E_3$	9.8 GPa	13.4 GPa
G_{23}	3.2 GPa	4.3 GPa
$G_{12} = G_{13}$	6.1 GPa	9.2 GPa
ν_{23}	0.55	0.55
$\nu_{12} = \nu_{13}$	0.37	0.37
α_1	0.18x10$^{-6}/°C$	0.18x10$^{-6}/°C$
$\alpha_2 = \alpha_3$	23.4x10$^{-6}/°C$	19.8x10$^{-6}/°C$
G_{IC}	227 Jm^2	145 Jm^2

Table 3.2 Thermoelastic properties of IM7/977-3 at cryogenic, room, and elevated temperature[10]

	IM7/977-3		
Temperature, $°C$	-196	23	150
E_1, MPa	182	180	180
E_2, MPa	11.7	9.7	6.9
G_{12}, GPa	9.2	6.1	5.5
ν_{12}	0.33	0.33	0.35
α_1,$10^{-6}/°C$	0.18	0.18	0.18
α_2,$10^{-6}/°C$	20.4	23.4	23.4
Transverse Tensile Strength, MPa	97.3	75.1	70.3
Curing free stress temp., $°C$		163	

3.2 Finite Element Analysis of Bulge Test

The bulge test was investigated using a two dimensional ANSYS model. A linear elastic orthotropic material model was used with the IM7/977-3 properties listed in Table 3.1. ANSYS element SHELL99 was selected. SHELL99 is a two dimensional layered element. The thickness and orientation of each ply were incorporated into the model. A 1.5in diameter circular balanced symetric composite plate with a [0/-45/90/45/$0_{0.5}$]$_S$ layup and plies of 0.00416in thick was subjected to a transverse pressure load across its face. Two different boundary conditions were modeled: simply supported and fixed. The boundary condition was applied to the nodes along the circumference of the circle.

To compare the results, the finite element data for the fixed and simply supported cases was plotted alongside the experimental data taken using a strain gage bonded to the center of a bulge test specimen with the same layup and material properties used with the finite element analysis. The finite element data was compiled by isolating the elements that would correspond to the area under the strain gage. The values for strain and deflection were then tabulated and averaged to obtain strain and deflection values. Figure 3.1 shows the pressure as a function of transverse deflection, and Figure 3.2 shows the average strain as a function of the transverse deflection. Figure 3.2 shows that the strain reported from the simply supported model most closely predicts the strains reported from the experimental data. One aspect of Figure 3.1 is the non-linearity of the experimental data. A possible reason for this behavior is the boundary conditions of the bulge fixture. The clamp has a small radius where it meets the specimen. This radius may cause the pressure to increase

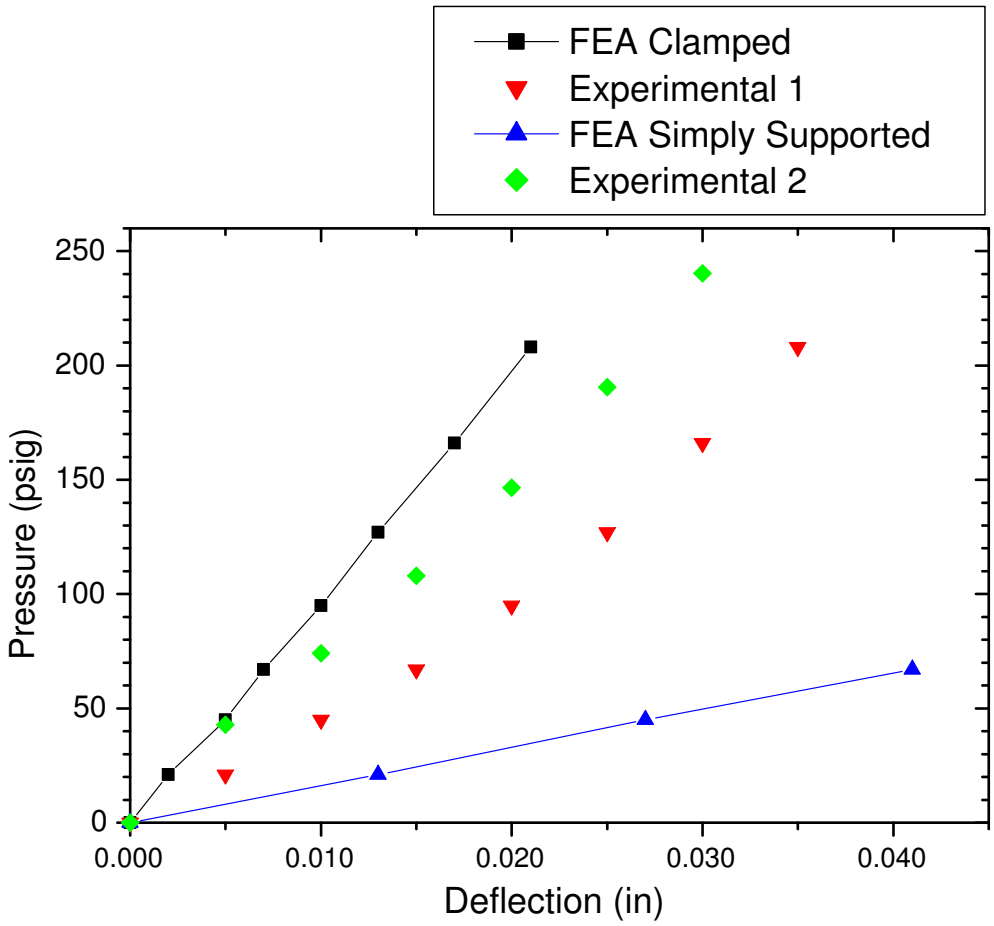

Figure 3.1 Pressure versus deflection comparison between FEA and experimental results

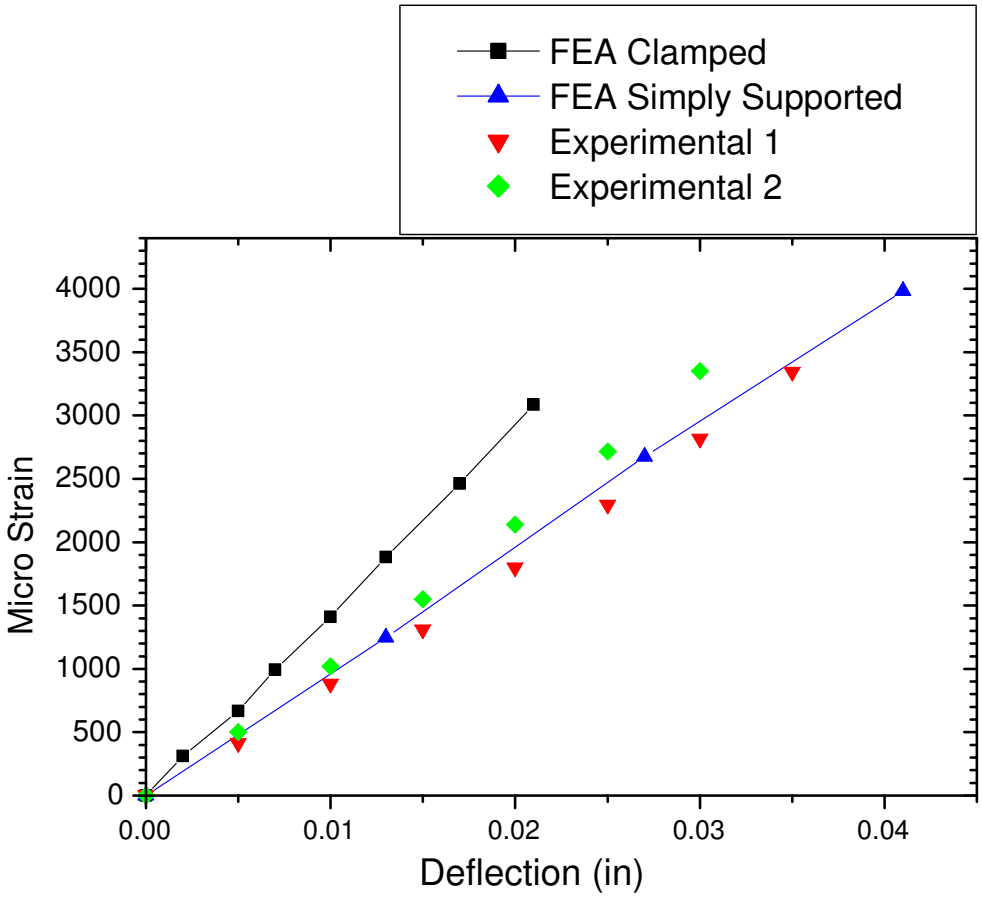

Figure 3.2 Strain versus deflection comparison between FEA and experimental results

as the specimen comes in contact with it at higher deflections. Figure 3.3 is a section view of the bulge fixture that illustrates this concept. More extensive modeling is needed to

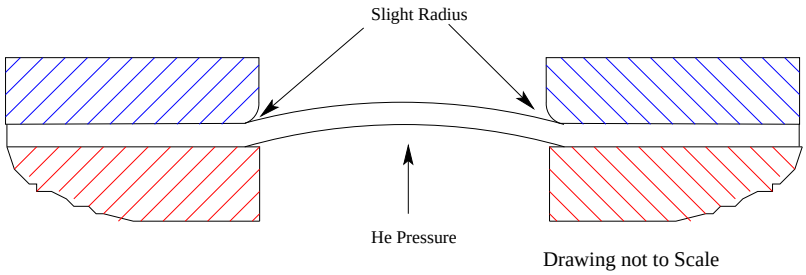

Figure 3.3 Cut away section showing the bulge test specimen clamped in the bulge fixture

generate a better correlation between the numerical data and the experimental data. The most probable reason for the differences between the model and the experimental data is the boundary conditions. The real conditions have an elastic boundary condition that lies somewhere between simply supported and fixed. Elastic boundary conditions would need to be included in the FEA analysis to better approximate the real conditions.

3.3 Stress Induced During the Bulge Test

The stress induced during the bulge test can be determined experimentally using a biaxial strain gage bonded to the center of the bulge test specimen and classical laminate plate theory. Assuming that the specimen is under membrane behavior with no bending

moments and that there is no shear strain in the specimen, the strain in the laminate is given in Equation 3.1

$$\epsilon_o = \begin{bmatrix} \epsilon_x \\ \epsilon_y \\ 0 \end{bmatrix} \mu\epsilon \tag{3.1}$$

where ϵ_x and ϵ_y are the strains measured from the bulge test. The stress in each ply in laminate axes given in Equation 3.2 is found using Hooke's Law

$$\sigma_i^L = E(-\theta)\epsilon_o \tag{3.2}$$

where $E(-\theta)$ is the ply stiffness tensor rotated through a negative ply angle. The stress in each ply in ply axes is given by Equation 3.3 and is found by multiplying the stress in each ply in laminate axes by the transformation matrix.

$$\sigma_i^P = T(\theta)\sigma_i^L \tag{3.3}$$

The ply stress can then be used in a failure criterion or compared to stress values given by other researchers.

This methodology was applied to the experimental data shown by Experimental 1 in Figure 3.1 and Figure 3.2. Table 3.3 lists the membrane stress in each ply for 0.025in of deflection. Due to symmetry, only half of the laminate plies are shown.

Table 3.3 Ply stress for an IM7/977-3 hand layed specimen for a 0.025in deflection

Ply	σ_x (MPa)	σ_y (MPa)	σ_{xy} (MPa)
0	521	37	0
-45	499	38	2
90	477	39	0
45	499	38	-2
0	521	37	0

CHAPTER IV

EXPERIMENTAL

4.1 Bulge Testing Proceedure

A bulge test is conducted by first cutting the sample from a panel. Each composite lot is fabricated in an 8in x 4in panel. Figure 4.1 shows how the composite panel is sectioned. Eight 2in x 2in specimens are cut using a diamond sectioning saw. During early

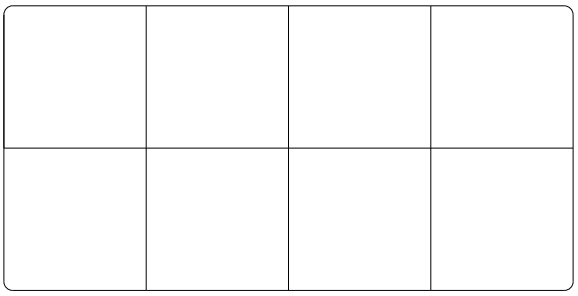

Figure 4.1 Composite panel schematic

bulge testing, the corner specimens were found to show drastically increased leak rates in the undamaged condition. The corner pieces are set aside to use for determining volume fraction and density which will be discussed in Section 4.2. After the specimen has been selected, it can be installed in the bulge fixture. The Teflon O-Ring that seals between the composite sample and the fixture is replaced prior to each test when centering

the specimen over the pressure chamber. The sample and the Teflon O-Ring can be seen in Figure 2.2. After centering the specimen, the clamp is placed over the specimen and the bolts are torqued to 41in-lb using a torque wrench. The next step is to determine the pressure needed to bulge the specimen 0.025in at the center. A dial indicator is mounted to the fixture and the pressure is adjusted until the indicator reads 0.025in. This can be seen in Figure 4.2 . This pressure will be used for every decay test on this specimen. Figure 4.3

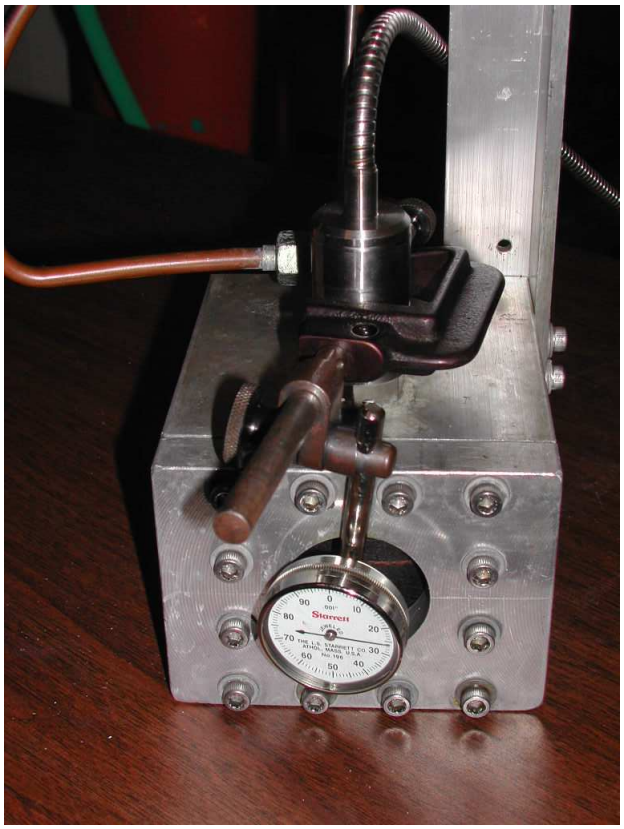

Figure 4.2 Determining the pressure from deflection for a bulge test

shows the fixture in a water bath. The water bath eliminates temperature fluctuations that can affect the pressure reading. Plastic sheeting prevents the water from contaminating

Figure 4.3 Bulge test fixture submerged in a water bath

the specimen and pressure transducer. Once the test fixture temperature reaches equilibrium with the water bath temperature, which takes about an hour, five pressure decay runs are measured to determine the decay rate for an untreated specimen. The fixture is re-pressurized between each cycle. The fixture is then submerged in liquid nitrogen. Figure 4.4 shows the fixture in a LN_2 bath. After about 15 min, the fixture reaches thermal

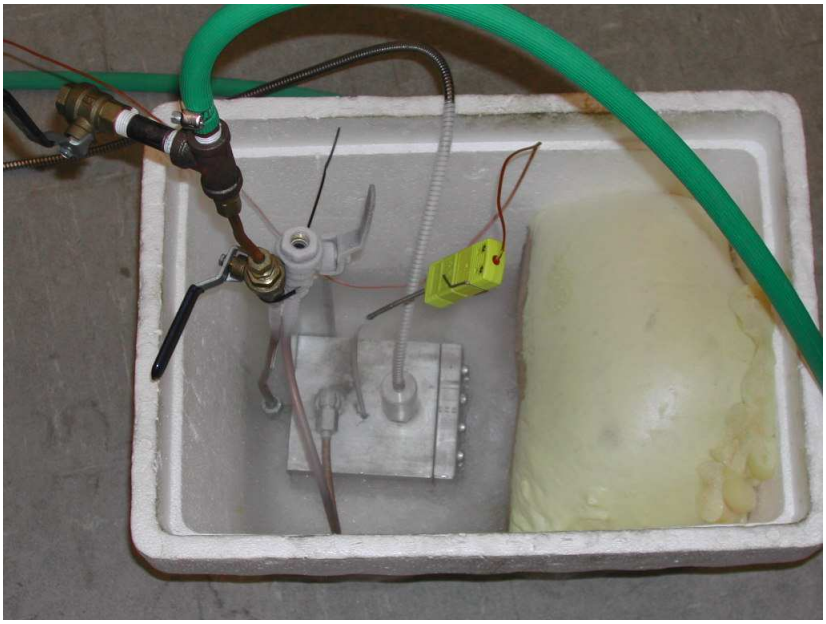

Figure 4.4 Bulge test fixture submerged in LN_2

equilibrium and the pressure is cycled 75 times. The pressure is applied for two seconds during each cycle with a 1 second delay between application. After cycling the specimen, the fixture is removed from the LN_2 and allowed to reach room temperature. The fixture is then submerged in the water bath so five more decay runs can be collected. The data is then collected and organized into data sheets shown Appendix A.

4.2 Density and Volume Fraction

For each sample lot fabricated in the laboratory, density and fiber volume fraction are recorded. Density was measured using a ED-120T electronic densimeter. The fiber volume fraction was calculated using optical microscopy. First a section of the composite sample was sectioned and mounted in Epofix epoxy. After curing, the sample was ground using 220 grit sandpaper followed by a $15\mu m$ diamond suspension. The sample was then polished using a $3\mu m$ diamond suspension. Once polished, optical micro-graphs were taken of the plies that lay perpendicular to the micro-graph. Figure 4.5 is an optical micro-graph of a section of B002 that was used to calculate the volume fraction. The micrographs are taken using an 80x objective and recorded using a Polaroid picture. Using Equation 4.1 and a small grid, the fiber volume fraction can be calculated.

$$VF = \frac{(\text{Number of fibers})(\text{Fiber cross sectional area})}{\text{Total area of grid}} \tag{4.1}$$

Five different measurements are taken at random points on the micro-graph and averaged together to produce the fiber volume fractions.

4.3 Tensile Testing

Tensile testing was conducted in order to evaluate the quality of our layups and to possibly detect changes in the mechanical properties after adding clay modifiers to the resin. Testing was conducted on an Instron 8500 servo-mechanical load frame. Test parameters were selected to adhere to the ASTM D3039 standard for tensile testing polymer matrix

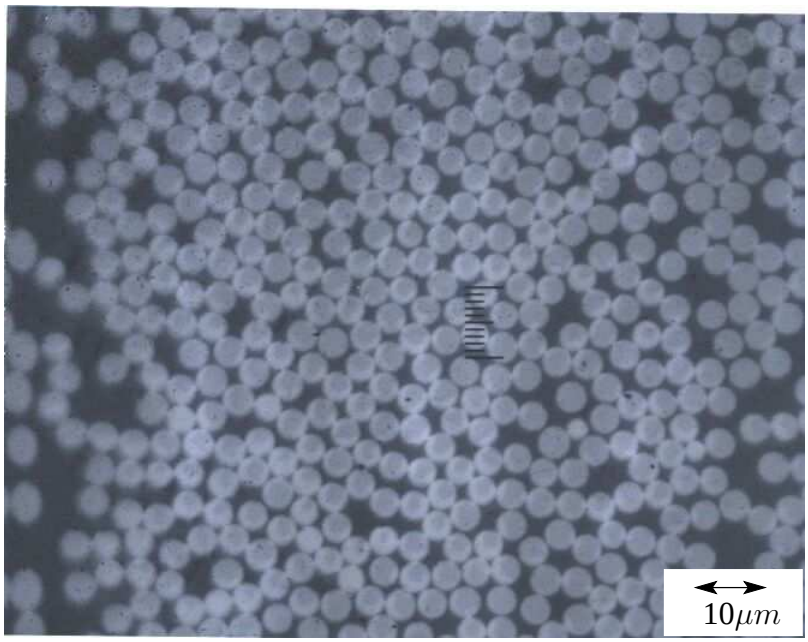

Figure 4.5 Optical micro-graph used for volume fraction calculations

composites. Each 8”x4” panel was sectioned into 8”x0.5” tensile bars using a diamond sectioning saw. G10 fiberglass end tabs were bonded to the grip section of the tensile bars using Hysol 9394 structural adhesive. Figure 4.6 shows the dimensions and geometry of the grip tabs. Table 4.1 shows the material types and the number of samples that will be tensile tested.

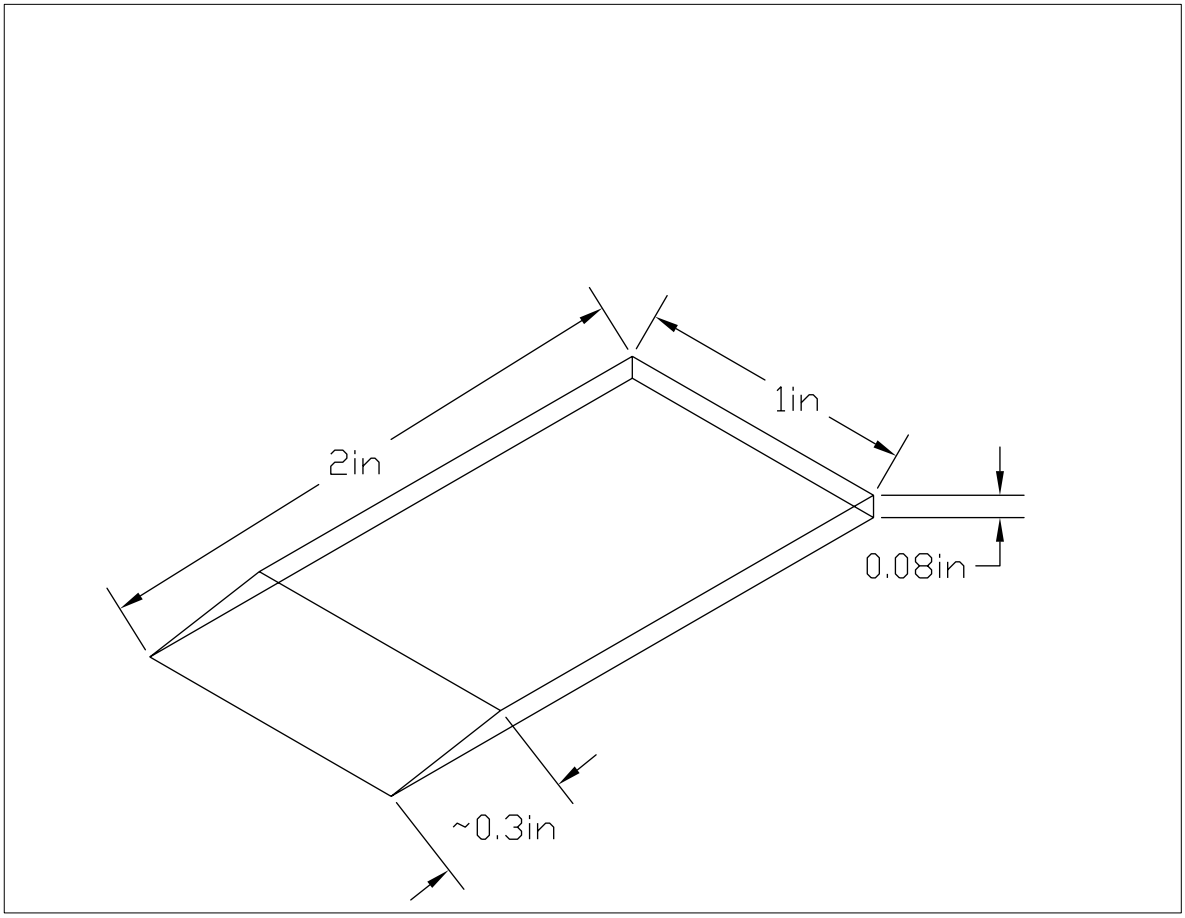

Figure 4.6 Schematic of grip tabs for tensile tests

Table 4.1 Room temperature tensile tests

Sample Code	Material Type	Number of Samples
A	IM7/977-3 hand layup from pre-preg fibers	8
B	IM7/977-3 wet layup	8
C	AS4/PEEK hand layup from pre-preg fibers	8
D	IM7/977-3/Clay modifier wet layup	8

CHAPTER V

RESULTS AND DISCUSSION

The bulge test method, developed in the previous chapters, is being used to screen the cryogenic performance of IM7/977-3 hand layup, IM7/977-3 wet layup, IM7/977-3 wet layup with various weight percents of clay additives, and AS4/PEEK hand layup. These material types will be designated A, B, C, and D as shown in Table 5.1. Each material type has a balanced symmetric layup with a stacking sequence of [0/-45/90/45/$0_{0.5}$]$_S$. Each

Table 5.1 Specimen type code designations

Specimen Type	Sample Code
IM7/977-3 Hand Layup	A
IM7/977-3 Wet Layup	B
AS4/PEEK Hand Layup	C
IM7/977-3/% Clay Wet Layup	D

bulge test specimen is given a test number made of the specimen type code, the lot number, and the individual specimen number. For example, the first specimen of lot one of a hand layup of IM7/977-3 would be designated as A001.1. These test code numbers can be seen on each of the test sheets in Appendix A and each tensile bar in Tables A.5, A.6, and A.7.

5.1 Results

5.1.1 Bulge Test Results

The bulge test sheets shown in Section **??** of the Appendix are used in Figure 5.1 to plot the corrected slope of each test. For each test, the transverse deflection of the specimen is set to 0.025in. This means that the pressures are not the same for all the specimens due to small variations in thickness, material properties, and layup quality. The intercepts have been adjusted to make all the slopes intercept the Y axis at 180psia so all the slopes can be compared.

5.1.2 Tensile Test Results

Table 5.2 presents a summary of the tensile data that has been collected. The data for the individual samples can be found in Section **??** of the Appendix.

Table 5.2 Tensile test results for A, B, and C samples

Sample Code		UTS (ksi)	Modulus (ksi)	Elongation %	Width	Thickness
A	Mean	143	11692.8	2.42%	0.4606	0.0420
	Std. Deviation	2.44	1620.84	0.12%	0.0026	7.59E-4
	COV	1.7%	13.9%	5.01%	0.56%	1.81%
B	Mean	128	10406	2.35%	0.4486	0.0458
	Std. Deviation	7.37	307.18	0.30%	0.0043	0.0006
	COV	5.77%	2.95%	12.92%	0.96%	1.32%
C	Mean	115	8136.1	1.496%	0.4825	0.0476
	Std. Deviation	9.26	79.84	0.242%	0.0032	0.0013
	COV	8.0%	1.0%	16.2%	0.7%	2.8%

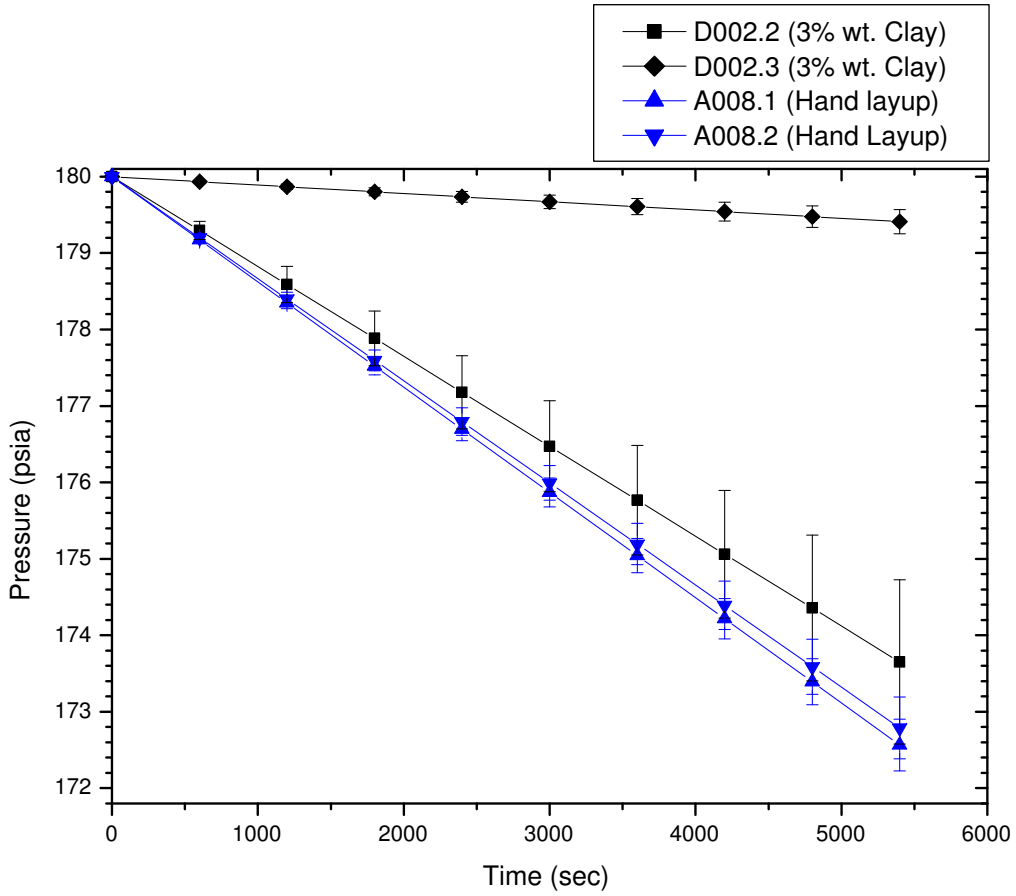

Figure 5.1 Current bulge test data for IM7/977-3 hand layup and IM7/977-3/3 wt% clay wet layup

5.1.3 Density and Fiber Volume Fraction

Table 5.3 lists the average density and the fiber volume fraction for the composite samples that have been fabricated. The density and fiber volume fraction for each sample is listed in Section **??** of the Appendix.

Table 5.3 Volume fraction and density values for the current A, B, C, and D samples

Sample Code		Density (gm/cc)	Fiber Volume Fraction	Wt% Clay
A	Mean	1.617	0.65	
	Std. Deviation	0.011	0.028	
	COV	0.68%	4.31%	
B	Mean	1.588	0.64	
	Std. Deviation	0.027	0.028	
	COV	1.70%	4.38%	
C	Mean	1.525	0.65	
	Std. Deviation	0.023	0.035	
	COV	1.51%	5.38%	
D	Mean	1.588	0.68	3%
	Std. Deviation	N/A	N/A	3%
	COV	N/A	N/A	3%

5.2 Discussion

5.2.1 Bulge Tests

Inspecting Figure 5.1, there is only a 3% difference in the slope of A008.1 and A008.2 with uncertainties of 4.6% and 5.6% respectively. The slope of D002.2 is 12% less than the A samples, but had a greater uncertainty of 17%. With the greater uncertainty of D002.2,

it is not possible to draw a conclusion whether there is a difference between it and the A samples. D002.3 has about 10% of the slope of D002.2. This large difference between D002.2 and D002.3 shows the inherent variability of the decay testing. More samples need to be tested to determine the decay rate.

5.2.2 Density and Fiber Volume Fraction

Composite properties are highly dependent on processing. Density and fiber volume fraction were recorded in order to ensure that the manufacturing process is producing quality composites. Also any commercial application will use a pre-impregnated fiber. In order to add clay modifiers in the lab, a wet lay-up is needed. Comparing the B samples to the A samples will show the differences between the wet lay-up and the hand lay-up using pre-pregs. From Tables A.8 and A.9, the density of the B samples is 2% less than that of the A samples. The volume fractions are comparable. No differences can be determined because the difference between the means falls within the standard deviation of the measurements. The D samples appear comparable to the B samples, although more samples are needed.

5.2.3 Tensile Tests

Tensile tests were conducted for the same reasons as listed in Section 5.2.2. Looking at Tables A.5 and A.6 the modulus for the A and B samples are comparable. Both means fall within the standard deviation of the two values. The ultimate tensile strength of the B

samples is 10% less than the A samples however. The AS4/PEEK samples fall below the IM7/977-3 in UTS, modulus, and elongation.

CHAPTER VI

SUMMARY

Different factors are cited in the current literature for improving the cryogenic performance of carbon fiber composites. Some of these include changing the T_g of the resin, changing the fiber modulus, adding nano scale modifiers, adding rubber modifiers, changing from a TS to a TP resin, and changing the layup sequence of the composite. A standard test bed is needed to evaluate how the different changes effect the cryogenic performance of the composite. In this study, four different composite formulations are studied: IM7/977-3 hand layup, IM7/977-3 wet layup, AS4/PEEK hand layup, and IM7/977-3/%wt clay additive wet layup. Each sample is characterized using room temperature tensile tests, fiber volume fraction, density, cryogenic bulge test. The bulge test fixture developed for this study was designed to rapidly screen composite for cryogenic performance. It was designed to test small scale specimens that could be easily fabricated in the laboratory. Promising formulations can then be more intensely studied using more expensive methods such as the NASA bulge test experiment or cryogenic tank fabrication.

BIBLIOGRAPHY

[1] X-33 Liquid Hydrogen Tank Test Investigation Team. Final report of the x-33 liquid hydrogen tank test investigation team. Technical report, George C. Marshall Space Flight Center, May 2000.

[2] Takahira Aoki, Takashi Ishikawa, Hisashi Kumazawa, and Yoshiki Morino. Mechanical performance of CF/Polymer composite laminates under cryogenic conditions. *Collection of Technical Papers - AIAA/ASME/ASCE/AHS/ASC Structures, Structural Dynamics and Materials Conference,*, 1(2):1448–1455, 2000.

[3] John F. Timmerman, Brian S. Hayes, and James C. Seferis. Cryogenic microcracking of nanoclay reinforced polymeric composite materials. *47th International SAMPE Symposium*, pages 2303–2311, May 2002.

[4] P. K. Mallick. *Fiber Reinforced Composites: Materials Manufacturing and Design*. Marcel Dekker, 1993.

[5] Daniel S. Adams, David E. Bowles, and Carl T. Herakovich. Thermally induced transverse cracking in graphite-epoxy cross-ply laminates. *Journal of Reinforced Plastics and Composites*, 5:152–169, July 1986.

[6] Cecelia H. Park and Hugh L. McManus. Thermally induced damage in composite laminates: Predictive methodology and experimental investigation. *Composites Science and Technology*, 56:1209–1219, 1996.

[7] Jae Noh, J. Whitcomb, B. Oh, D. Lagoudas, K. Maslov, A. Ganpatye, and V. Kinra. Numerical modeling, thermomechanical testing, and NDE procedures for prediction of microcracking induced permeability of cryogenic composites. *Fifth Conference on Aerospace Materials, Processing, and Environmental Technology (AMPET)*, September 16-18 2002.

[8] Brian J. Knouff, Stephen S. Tompkins, and N. Jayaraman. The effect of graphite fiber properties on microcracking due to thermal cycling of epoxy-cyanate matrix laminates. *ASTM STP 1230*, pages 268–282, 1994.

[9] Kevin H. Rivers, Joseph G. Sikora, and Sankara N. Sankaran. Detection of microleaks through complex geometries under mechanical load and at cryogenic temperatures. *Collection of Technical Papers - AIAA/ASME/ASCE/AHS/ASC Structures, Structural Dynamics and Materials Conference*, 1:312–322, 2001.

[10] Ran Y. Kim, Brian P. Rice, and Steven L. Donaldson. Microcracking in composite laminates under thermal environments: 150 to -196c. *47th International SAMPE Symposium*, pages 833–842, 2002.

[11] Hisashi Kumazawa, Takahira Aoki, and Ippei Susuki. Analysis and experiment of gas leakage through composite laminates for propellant tanks. *AIAA Journal*, 41(10):2037–2044, 2003.

[12] Hugh L. McManus and Jason R. Maddocks. On microcracking in composite laminates under thermal and mechanical loading. *Polymers I& Polymer Composites*, 4:305–314, 1996.

[13] Matthiew Nobelen, Brian S. Hayes, and James C. Seferis. Cryogenic cycling of carbon fiber/epoxy composites: Effects of matrix modification. *47th International SAMPE Symposium*, pages 1539–1549, 2002.

[14] G. A. Schoeppner, R. Kim, and S. L. Donaldson. Steady state cracking of pmcs at cryogenic temperatures. *Collection of Technical Papers - AIAA/ASME/ASCE/AHS/ASC Structures, Structural Dynamics and Materials Conference*, 1:296–306, 2001.

[15] Vernon T. Bechel, Mark B. Fredin, Steven L. Donaldson, Ran Y. Kim, and John D. Camping. Combined cryogenic and elevated temperature cycling of carbon / polymer composites. *47th International SAMPE Symposium*, pages 808–819, May 2002.

[16] John F. Timmerman, Matthew S. Tillman, Brian S. Hayes, and James C. Seferis. Low temperature behavior of carbon fiber/epoxy composites: Matrix and fiber influences on cryogenic microcracking. *46th International SAMPE Symposium*, pages 2303–2311, May 2001.

[17] Joseph D. Keenan and James C. Seferis. Effects of moisture and stoichiometry on the dynamic mechanical properties of a high-performance structural epxoy. *Journal of Applied Polymer Sciences*, 24:2375–2387, 1979.

[18] Sabyasachi Ganguli, Derrick Dean, Kelvin Jordan, Gary Price, and Richard Vaia. Mechanical properties of intercalated cyanate ester-layered silicate nanocomposites. *Polymer*, 44:1315–1319, 2003.

[19] Thomas J. Pinnavaia, Tie Lan, Zhen Wang, Hengzhen Shi, and P. D. Kaviratna. Clay-reinforced epoxy nanocomposites: Synthesis, properties, and mechanism of formation. In G. M. Hcow and K. E. Gonsalves, editors, *Nanotechnology*, ACS Symposium, chapter 17, pages 251–261. American Chemical Society, Washington, DC, 1996.

[20] G. Hartwig. Low temperature ductile matrices for advanced fiber composites. In Gu?nther Hartwig and David Evans, editors, *Nonmetallic materials and composites at low temperatures*, volume 3 of *Cryogenic Materials Series*, pages 153–150, New York, 1984. Plenum Press.

[21] J. Lee, R. Patton, J. Schneider, C. Pittman Jr., J. Ragsdale, L. Wang, and A. T. Nettles. Thermoplastics for use in cryogenic composite fuel tanks. *49th International SAMPE Convention*, May 2004.

[22] Y. S. Toulokian. *Thermophysical Properties of Matter*, volume 13. IFI/Plenum, 1977.

[23] G. Hartwig, H. Jager, and S. Knaak. Interlaminar shear strength of carbon-fibre reinforced thermoplastics polycarbonate and polysulfone. In Gu?nther Hartwig and David Evans, editors, *Nonmetallic materials and composites at low temperatures*, volume 3 of *Cryogenic Materials Series*, pages 167–175, New York, 1984. Plenum Press.

[24] Alan T. Nettles and Emily J. Biss. Low temperature mechanical testing of carbon-fiber/epoxy-resin composite materials. Technical report, NASA Marshall Space Flight Center, 1996.

[25] Hugh W. Coleman and Glenn W. Jr. Steele. *Experimentation and Uncertainty Analysis for Engineers*, chapter 7, pages 208–209. John Wiley and Sons, Inc., 1999.

[26] Hugh W. Coleman and Glenn W. Jr. Steele. *Experimentation and Uncertainty Analysis for Engineers*, chapter 2, pages 27–41. John Wiley and Sons, Inc., 1999.

[27] Hugh W. Coleman and Glenn W. Jr. Steele. *Experimentation and Uncertainty Analysis for Engineers*. John Wiley and Sons, Inc., 1999.

APPENDIX A

TEST DATA

Table A.1 Bulge Test Data Sheet for D002.2

Slopes and Regression Uncertainty						**D002.2**
Run Number	Untreated (psi/sec)	S_m (psi/sec)	Uncertainty Percentage	Cryo1 (psi/sec)	S_m (psi/sec)	Uncertainty Percentage
1	-6.377E-05	4.761E-07	0.75%	-9.358E-04	4.825E-07	0.05%
2	-4.389E-05	5.168E-07	1.18%	-1.243E-03	7.820E-07	0.06%
3	-1.597E-05	4.820E-07	3.02%	-1.553E-03	1.386E-06	0.09%
4	-3.893E-05	4.548E-07	1.17%	-1.197E-03	1.155E-06	0.10%
5	-4.565E-05	5.354E-07	1.17%	-1.158E-03	7.739E-07	0.07%
Mean	-4.164E-05			-1.217E-03		
Stdev	1.716E-05			2.216E-04		
COV	41.20%			18.21%		
Uncertainty	1.535E-05			1.982E-04		
Corrected Slope	-1.176E-03	(psi/sec)				
Uncertainty	1.988E-04	(psi/sec)				

Table A.2 Bulge test data sheet for D002.3

Slopes and Regression Uncertainty						**D002.3**
Run Number	Untreated (psi/sec)	S_m (psi/sec)	Uncertainty Percentage	Cryo1 (psi/sec)	S_m (psi/sec)	Uncertainty Percentage
1	-1.16E-04	2.379E-05	20.50%	-1.85E-04	4.591E-07	0.25%
2	-7.58E-05	4.734E-07	0.62%	-1.74E-04	4.605E-07	0.26%
3	-8.10E-05	5.612E-07	0.69%	-2.19E-04	4.636E-07	0.21%
4	-1.08E-04	5.428E-07	0.50%	-1.99E-04	4.771E-07	0.24%
5	-4.50E-05	4.640E-07	1.03%	-1.96E-04	4.499E-07	0.23%
Mean	-8.515E-05			-1.946E-04		
Stdev	2.824E-05			1.664E-05		
COV	33.17%			8.55%		
Uncertainty	2.526E-05			1.488E-05		
Corrected Slope	-1.095E-04	(psi/sec)				
Uncertainty	2.932E-05	(psi/sec)				

Table A.3 Bulge test data sheet for A008.1

Slopes and Regression Uncertainty						**A008.1**
Run Number	Untreated (psi/sec)	S_m (psi/sec)	Uncertainty Percentage	Cryo1 (psi/sec)	S_m (psi/sec)	Uncertainty Percentage
1	-7.457E-05	4.382E-07	0.59%	-1.513E-03	6.377E-07	0.04%
2	-1.271E-04	4.959E-07	0.39%	-1.475E-03	1.196E-06	0.08%
3	-8.592E-05	4.663E-07	0.54%	-1.553E-03	1.388E-06	0.09%
4	-8.503E-05	5.346E-07	0.63%	-1.434E-03	1.154E-06	0.08%
5	-9.771E-05	4.539E-07	0.46%	-1.381E-03	1.009E-06	0.07%
Mean	-9.407E-05			-1.471E-03		
Stdev	2.021E-05			6.714E-05		
COV	21.48%			4.56%		
Uncertainty	1.808E-05			6.005E-05		
Corrected Slope	-1.377E-03	(psi/sec)				
Uncertainty	6.271E-05	(psi/sec)				

Table A.4 Bulge test data sheet for A008.2

Slopes and Regression Uncertainty **A008.2**

Run Number	Untreated (psi/sec)	S_m (psi/sec)	Uncertainty Percentage	Cryo1 (psi/sec)	S_m (psi/sec)	Uncertainty Percentage
1	-2.30E-04	4.831E-07	0.21%	-1.51E-03	6.374E-07	0.04%
2	-1.51E-04	4.375E-07	0.29%	-1.47E-03	1.195E-06	0.08%
3	-2.16E-04	4.926E-07	0.23%	-1.49E-03	7.028E-07	0.05%
4	-2.05E-04	5.328E-07	0.26%	-1.57E-03	5.765E-07	0.04%
5	-2.33E-04	4.694E-07	0.20%	-1.67E-03	5.611E-07	0.03%
Mean	-2.068E-04			-1.542E-03		
Stdev	3.309E-05			7.72E-05		
COV	16.00%			5.00%		
Uncertainty	2.960E-05			6.902E-05		

Corrected Slope	-1.335E-03	(psi/sec)
Uncertainty	7.510E-05	(psi/sec)

Table A.5 Tensile test data for IM7/977-3 hand layup using pre-preg fibers

Specimen	UTS (Ksi)	Modulus (ksi)	% Elongation	Width	Thickness
A104.4	151	11639.6	2.78%	0.4609	0.0425
A104.5	158	11716.2	3.13%	0.463	0.0425
A104.6	158	11285.6	3.32%	0.4577	0.0408
A103.1	142	14527.8	2.41%	0.4562	0.0423
A103.2	140	11255.7	2.35%	0.4626	0.0417
A103.3	143	11169.5	2.28%	0.4592	0.0408
A103.4	147	10402.7	2.60%	0.4625	0.0425
A103.5	143	11108.3	2.45%	0.4625	0.0425
Mean	143	11692.8	2.42%	0.4606	0.0420
Stdev	2.44	1620.84	0.12%	0.0026	7.59E-4
COV	1.7%	13.9%	5.01%	0.56%	1.81%

Table A.6 Tensile test data for IM7/977-3 wet layup

Specimen	UTS (Ksi)	Modulus (ksi)	% Elongation	Width	Thickness
B101.1	135	10621.4	2.43%	0.4427	0.0457
B101.2	118	9996.2	1.93%	0.4479	0.045
B101.3	128	10344.1	2.36%	0.4519	0.0464
B101.4	131	10660.8	2.66%	0.4517	0.0461
Mean	128	10406	2.35%	0.4486	0.0458
Stdev	7.37	307.18	0.30%	0.0043	0.0006
COV	5.77%	2.95%	12.92%	0.96%	1.32%

Table A.7 Tensile test data for AS4/PEEK hand layup using pre-preg fibers

Specimen	UTS (Ksi)	Modulus (ksi)	% Elongation	Width	Thickness
C101.1	124	7945	3.26%	0.4866	0.0490
C101.2	122	8320	2.24%	0.4849	0.0480
C101.3	116	8192	1.77%	0.4819	0.0471
C101.4	115	8193	1.67%	0.4802	0.0482
C101.5	100	8080	1.33%	0.4788	0.0455
Mean	115	8136.1	1.496%	0.4825	0.0476
Stdev	9.26	79.84	0.242%	0.0032	0.0013
COV	8.0%	1.0%	16.2%	0.7%	2.8%

Table A.8 Volume fraction and density values for the current A samples

Sample Number/ Designation	Density (gm/cc)	Fiber Volume Fraction	Wt% Clay
A001	1.614	0.66	
A002	1.617	0.64	
A003	1.601	0.66	
A004	1.606	0.69	
A005	1.629	0.67	
A006	1.627	0.68	
A007	1.623	0.62	
A008	1.629	0.63	
A009	1.608	0.61	
Average	1.617	0.65	
Stdev	0.011	0.028	
COV	0.68%	4.31%	

Table A.9 Volume fraction and density values for the current B samples

Sample Number/ Designation	Density (gm/cc)	Fiber Volume Fraction	Wt% Clay
B001	1.569	0.62	
B002	1.607	0.66	
Average	1.588	0.64	
Stdev	0.027	0.028	
COV	1.70%	4.38%	

Table A.10 Volume fraction and density values for the current C samples

Sample Number/ Designation	Density (gm/cc)	Fiber Volume Fraction	Wt% Clay
C001	1.508	0.62	
C002	1.541	0.67	
Average	1.525	0.65	
Stdev	0.023	0.035	
COV	1.51%	5.38%	

Table A.11 Volume fraction and density values for the current D samples

Sample Number/ Designation	Density (gm/cc)	Fiber Volume Fraction	Wt% Clay
D002	1.588	0.68	3%
Average	1.588	0.68	
Stdev	N/A	N/A	
COV	N/A	N/A	

APPENDIX B

BULGE TEST DESIGN

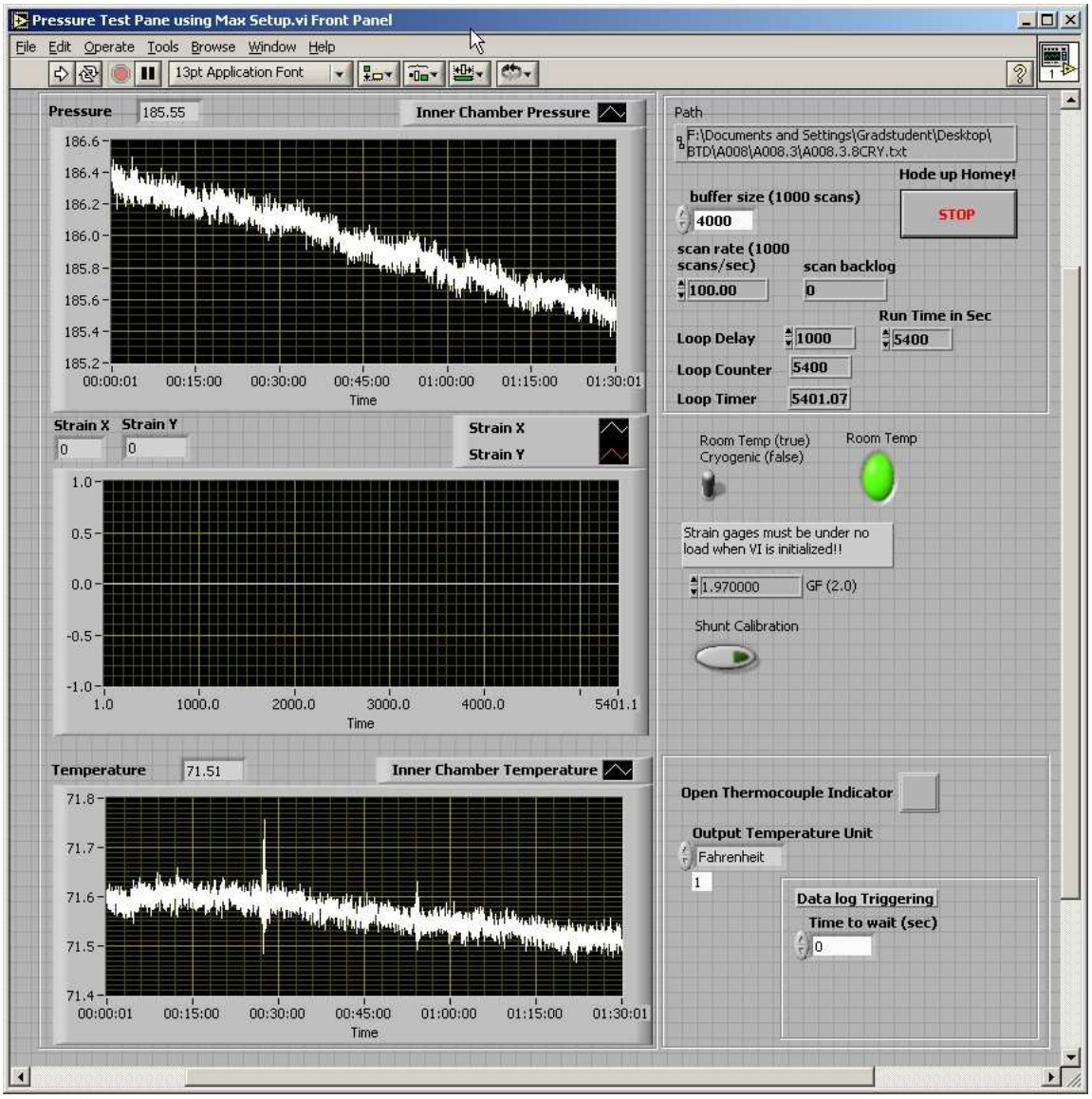

Figure B.1 LabView front panel screen capture

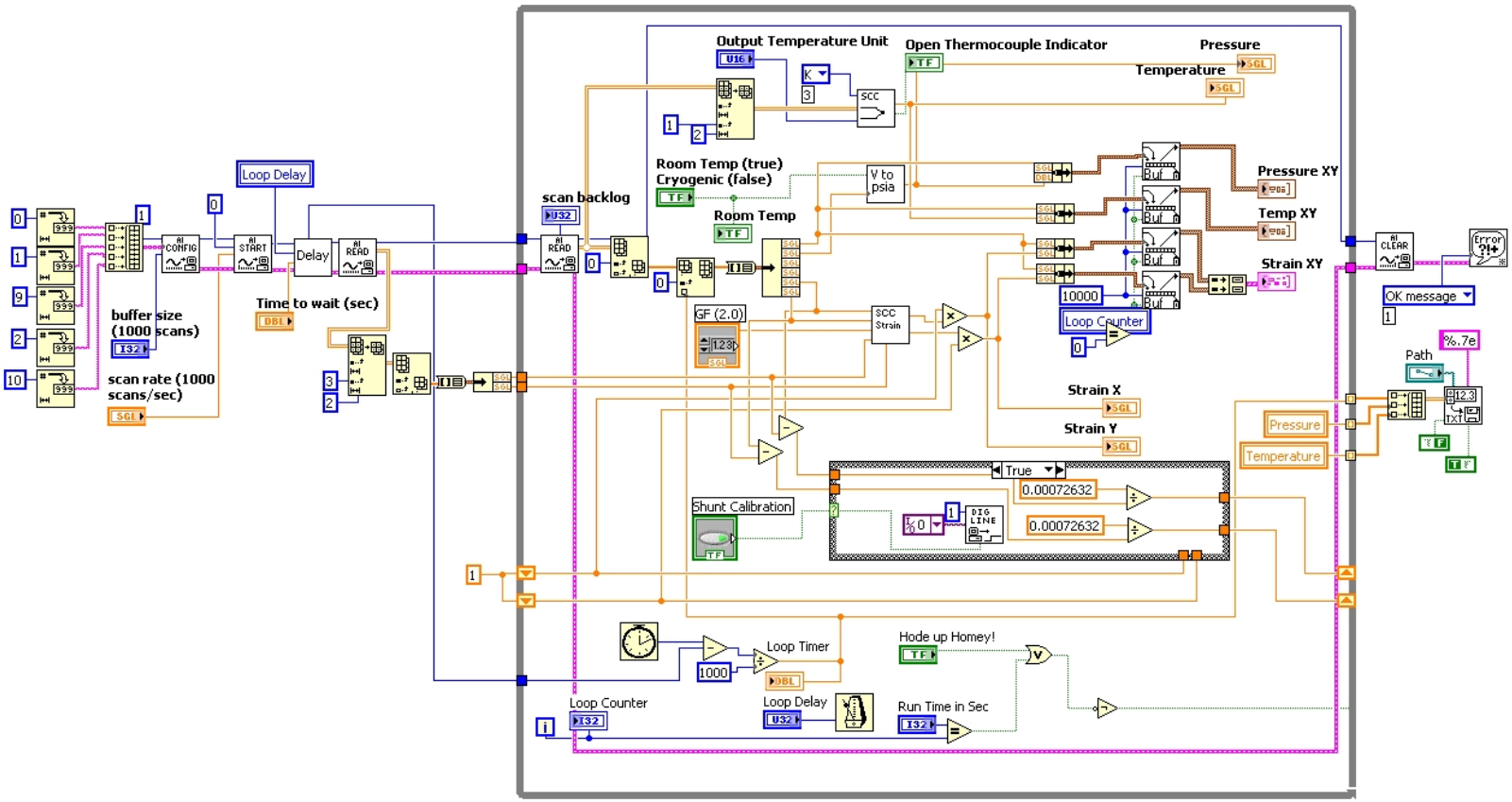

Figure B.2 LabView code

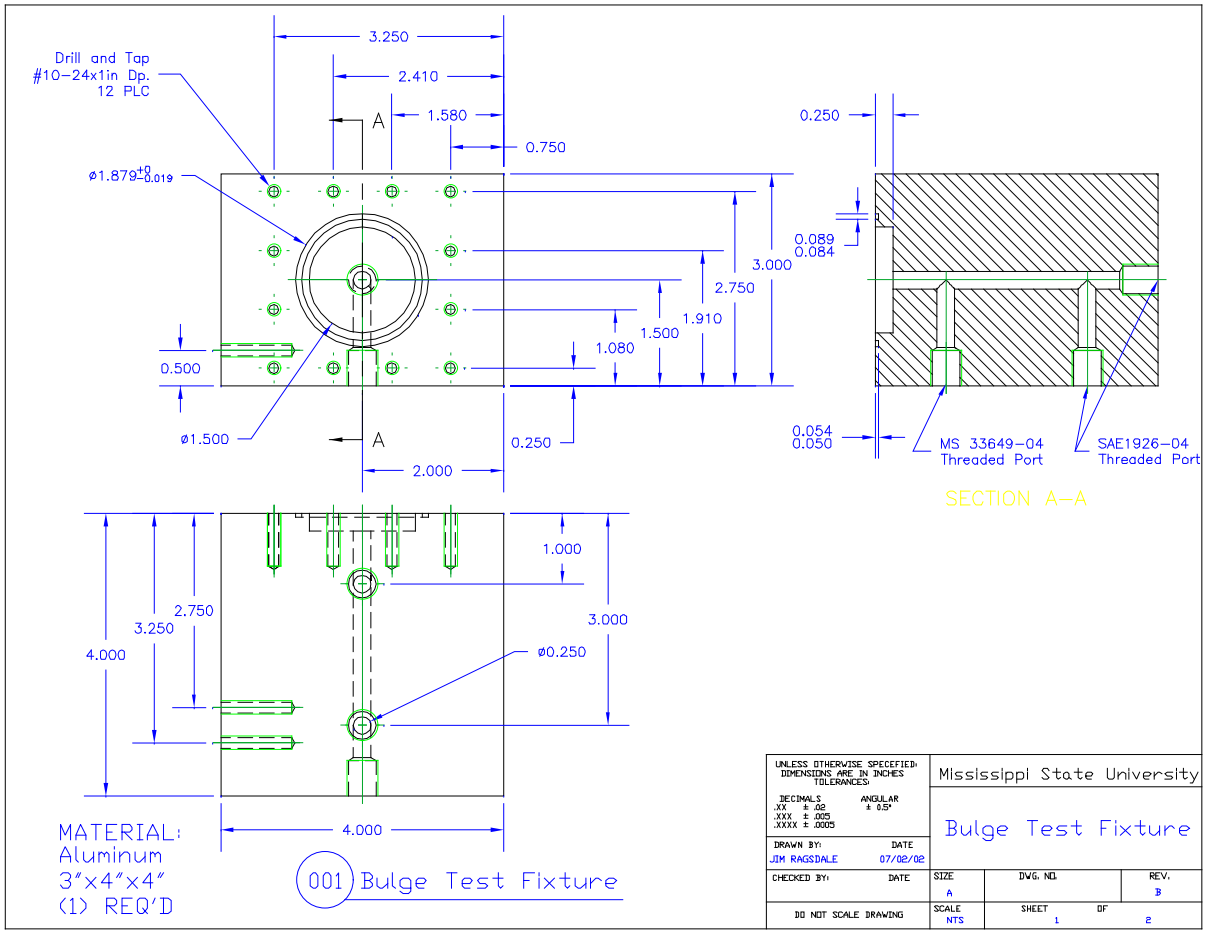

Figure B.3 Bulge test fixture body production drawing

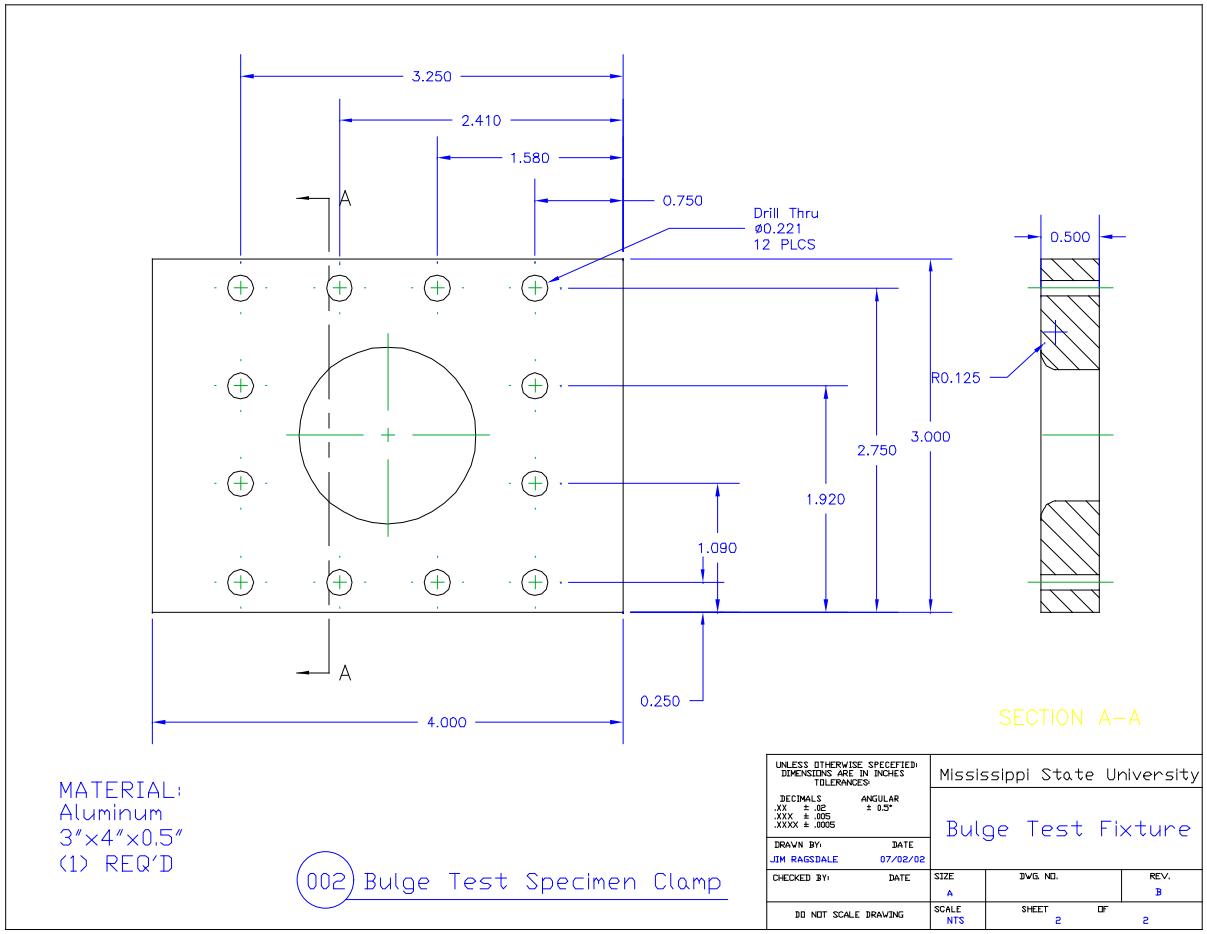

Figure B.4 Bulge test fixture clamp production drawing